DEVELOPMENTAL CHANGES IN THE IMMUNOLOCALIZATION OF THE SODIUM CALCIUM EXCHANGER AND THE RYANODINE RECEPTOR OF VENTRICULAR CARDIAC MYOCYTES

by

Perveen K Biln
BSc. Kinesiology, Simon Fraser University 2001

THESIS PROJECT SUBMITTED IN PARTIAL FULFILLMENT OF THE REQUIREMENTS FOR THE DEGREE OF

MASTER OF SCIENCE

In the
Department
of
Molecular Biology and Biochemistry

SIMON FRASER UNIVERSITY

Summer 2005

APPROVAL

Name: **Perveen Kaur Biln**

Degree: **Master of Science**

Title of Thesis: **Developmental Changes in the Immunolocalization of the Sodium Calcium Exchanger and the Ryanodine Receptor of Ventricular Cardiac Myocytes**

Examining Committee:

Chair: **Dr. David Vocadlo**
Associate Professor, Department of Molecular Biology and Biochemistry

---

Dr. Glen F. Tibbits
Senior Supervisor
Professor, School of Kinesiology

Dr. Bruce P. Brandhorst
Supervisor
Professor, Department of Molecular Biology and Biochemistry

Dr. Christopher T. Beh
Supervisor
Assistant Professor, Department of Molecular Biology and Biochemistry

---

Dr. Nancy Hawkins
Internal Examiner
Assistant Professor, Department of Molecular Biology and Biochemistry

Date Defended/Approved: July 28, 2005

SIMON FRASER UNIVERSITY

PARTIAL COPYRIGHT LICENCE

Simon Fraser University

Ethics Approval

The author, whose name appears on the title page of this work, has obtained human research ethics approval from the Simon Fraser University Office of Research Ethics for the research described in this work, or has conducted the research as a member of a project or course approved by the Ethics Office.

A copy of the approval letter has been filed at the Theses Office of the University Library at the time of submission of this thesis or project.

The original application for ethics approval and letter of approval is filed with the Office of Research Ethics. Inquiries may be directed to that Office.

Bennett Library
Simon Fraser University
Burnaby, BC, Canada

ABSTRACT

Excitation of adult mammalian heart plasma membrane (sarcolemma, SL) triggers the opening of L-type voltage-gated Ca^{2+} channels (DHPR), allowing Ca^{2+} to cross the SL and initiate release of Ca^{2+} stores from the sarcoplasmic reticulum (SR) via activation of the ryanodine receptor (RyR), a process termed calcium-induced-calcium release (CICR). The functional proximity of DHPR and RyR, which is essential to CICR, is not exhibited in neonate hearts. It has been proposed that NCX may contribute to Ca^{2+} influx via reverse mode activation during excitation-contraction (EC) coupling in neonate myocytes. To investigate if RyR activation from Ca^{2+}entry via reverse mode NCX is possible, we examined the colocalization of these two proteins during development. Changes in colocalization were examined using NCX and RyR immunolabelling and confocal microscopy. Deconvolved images of cardiomyocytes collected from rabbits 3-56-days old suggests the percentage of NCX colocalized with RyR increases in myocytes of 20- and 56-day old rabbits.

DEDICATION

To my husband Nick, for all the love and support

ACKNOWLEDGEMENTS

I would like to thank my supervisory committee, Dr. Glen Tibbits, Dr. Christopher Beh, and Dr. Bruce Brandhorst for the time and attention they devoted to my thesis. A special thank you to my senior supervisor, Glen Tibbits, for his mentorship, guidance and support, which has allowed me to grow both as a scientist and as an individual. This thesis would not have been completed if it were not for the assistance of my CMRL labmates, who shared their expertise and time along with their friendships. A special thanks to Jingbo Huang for teaching me myocyte isolations, Christian Marshall for all his advice over the years, and Haruyo Kashihara for all the help. I would like to extend my gratitude to the staff in the Kinesiology Main Office for treating me like a Kinesiology graduate student, even though I wasn't.

This experience has taught me many things, one of which is the value of friendship. Thank you to the girls in the Parkhouse lab, the Accilities, the Krieger Lab members and my friends at IHRE for the all the chats, coffee trips, lunches and laughs that have made this experience a memorable one. I would also like to thank Laura, for being such a great friend and confidant. My deepest thanks and love to my family who have always supported me in any direction I have chosen to go in life.

Lastly, I would like to thank my husband Nick for being my best friend, my cheering squad and for supporting me in everything I do.

TABLE OF CONTENTS

LIST OF FIGURES

LIST OF TABLES

CHAPTER 1:
INTRODUCTION AND REVIEW OF THE LITERATURE

1.1 Introduction:

Calcium (Ca^{2+}) is a vital and ubiquitous second messenger involved in the cellular signalling of many different tissues. In cardiac muscle, a rise in cytosolic Ca^{2+} is essential for initiating the cascade of cellular events leading to contraction. Excitation of cardiac muscle triggers the opening of L-type voltage-gated Ca^{2+} channels (DHPR), allowing Ca^{2+} to cross the plasma membrane or sarcolemma (SL). This calcium then initiates release of Ca^{2+} stores from the sarcoplasmic reticulum (SR) upon binding to the ryanodine receptor (RyR), in a process known as calcium-induced-calcium release (CICR). Ca^{2+} from both sources then binds to site II of troponin C, triggering a sequential cascade of macromolecular interactions that result in cardiac muscle contraction and force generation (Bers, 2001; Fabiato, 1983). The process of an action potential generating contraction is referred to as excitation-contraction (E-C) coupling (Figure 1). Relaxation is achieved by returning the cytosolic [Ca^{2+}] to resting levels (~100 nM) primarily in two ways: (1) the majority (60-90%) of Ca^{2+} is returned to the SR by the cardiac specific **S**arcoplasmic **E**ndoplasmic **R**eticulum **C**alcium **A**TPase (SERCA2a) and (2) almost all of the remaining Ca^{2+} is removed via the cardiac specific sodium calcium exchanger (NCX1.1) (Bers, 1991; Bers, 2001).

In adult myocytes, the SR Ca^{2+} release contributes the majority of the Ca^{2+} binding to troponin C (Balaguru et al., 1997; Bers, 2001; Fabiato, 1983). The

dependence on transsarcolemmal Ca^{2+} flux through the DHPR to trigger SR Ca^{2+} release necessitates a functional proximity (~ 20 nm) of the DHPR on the plasma membrane with the RyR of the SR which is made possible by the transverse (T)-tubule network (see Figure 1). T-tubules are organized, structural invaginations of the plasma membrane that occur at intervals of ~2.0 μm. They serve to increase the surface area of the cell and to provide a medium to facilitate exchange deep into the cytosol. However, at birth, myocytes do not have a T-tubule network; it begins to develop during the post-natal period. We have previously shown that in rabbit neonatal hearts, DHPR and RyR colocalization is restricted to the cell periphery, becoming predominantly internal couplings during ontogeny. Changes in the degree of colocalization and the distribution pattern during development were consistent with increasing dependence on the adult phenotype of CICR and the onset of T-tubule development (Sedarat et al., 2004; Sedarat et al., 2000). This finding, along with other morphological and functional differences is suggestive of an alternate E-C coupling mechanism in neonate ventricular myocytes (Artman et al., 2000) (Balaguru et al., 1997) (Chin et al., 1990; Sedarat et al., 2000) (Huynh et al., 1992; Wetzel et al., 1993).

This project attempts to provide insight into neonate E-C coupling mechanisms, through examination of the changes that occurred in select structures and proteins involved in this process throughout post-natal development. Knowledge of the alterations in protein distribution and structure development may provide insight into the mechanisms underlying neonate E-C coupling and how these processes change with age.

1.2 Regulation of Myocardial Contractility in the Adult Myocardium

1.2.1 Morphology of Adult Ventricular Myocytes

Mammalian ventricular myocytes have an average length of 120 μm with a width of 20 μm. They are often binuclear, with the nuclei usually located toward the centre of the cell. Ventricular myocytes appear rod-shaped which is the result of its internal structure, which consists of rod-like myofibrils enclosed by the sarcolemma. Myofibrils are bundles of contractile proteins that run from one cell end to the other. The interposition of the various contractile proteins (i.e. actin, myosin, troponin, tropomyosin, and α-actin) gives the myofibril a repeating pattern of light and dark bands. One repeat of the pattern forms a sarcomere, which is the fundamental contractile unit (Bers, 2001; Sperelakis, 2001). Sarcomeres of mammalian ventricular myocytes are bounded by the Z-lines, contain the A-band and M-line and have a characteristic resting length of 2.2 μm, (Figure 2). Myofibrils have varying lengths and cross sectional profiles leading to the formation of staggered cell ends' which are the basis for the step-like profiles of the intercalated discs. Intercalated discs (ID) are specialized structures that serve as connections between adjacent myocytes. Regions within the ID, known as nexuses, contain gap junctions (predominately composed of connexion 43) that electrically couple cells, enabling the ventricles to function as a syncytium (Berne et al., 1998).

The major organelles of ventricular myocytes are the myofibrils and mitochondria, which occupy 44% and 35% of the cell volume respectively. The mitochrondria are identifiable due to their considerable opacity and tendency to lie in longitudinal rows between the myofibrils, although there is also a subsarcolemmal population. They are densely packed and substantially larger than in other cells; the areas

of the mitochrondrial respiratory membrane per unit volume is 16-fold greater than the volume occupied by the SR membrane, underscoring the high demand for ATP in these cells (Bers, 2001; Page, 1978; Sperelakis, 2001). The other major identifiable components of the adult ventricular myocyte are the nuclei, the intercalated discs and the plasma membrane. The plasma membrane can be subdivided into the external sarcolemmal envelope and the T-tubular system, both of which contain caveolae and dyadic junctional complexes with the terminal cisternae of the SR. The external sarcolemmal itself can also be further divided into the intercalated discs which are subdivided into gap junctions, fasciae adherentes, desmosomes (Page, 1978).

1.2.2 Cellular Components Important to Excitation–Contraction Coupling

E-C coupling is the process by which an electrical signal, membrane depolarization, is translated into the mechanical event of cell contraction. In cardiac muscle, the major players in this transduction are two calcium permeant channels: the DHPR, located primarily in the T-tubules of the plasma membrane and the ryanodine-sensitive ligand-gated SR calcium release channel, RyR.

The cardiac action potential is propagated along the plasma membrane, which is divided into the external envelope and the T-tubular system. T-tubules are invaginations of the plasma membrane that intertwine and surround the myofibrils. The tubules branch and anastomose to form highly organized structures that lie specifically at the Z-lines of the sarcomeres, such that each is flanked by a tubule. Each tubule is associated with a single expanded cistern of the SR to form the aforementioned dyads, which enables simultaneous excitation along the width of a myocyte. The lumina of T-tubules are continuous with the bulk interstitial fluid creating short diffusion distances for the rapid

exchange of oxygen, carbon dioxide, substrates and waste material between the myocytes and the capillary system (Berne et al., 1998; Bers and Stiffel, 1993).

The sarcoplasmic reticulum (SR) is the major Ca^{2+} storage site of ventricular myocytes. The SR is an entirely intracellular membrane network that surrounds the cell's contractile apparatus and can be divided in to two parts, junctional and corbular. Junctional SR consists of expanded elements that form connections with the sarcolemma and / or T-tubules, while corbular SR contains more narrow elements that run along the myofibrils and do not interact with the plasma membrane (Berne et al., 1998; Page, 1978; Schaart et al., 1997). The SR has a high capacity for Ca^{2+} storage due to the presence of calcium-binding proteins such as calsequestrin in its luminal cavity and it is responsible for releasing the majority of Ca^{2+} binding to myofilaments (Williams, 1997). SR Ca^{2+} release is linked to membrane depolarization by the functional interaction of the DHPR with the RyR at specialized intracellular junctions known as dyads (Flucher and Franzini Armstrong, 1996)

A dyad is the structure formed by the apposition of a terminal cisterna of the junctional SR to a short T-tubule segment (Flucher and Franzini Armstrong, 1996; Franzini-Armstrong et al., 1999). This close apposition enables the functional coupling of DHPR and RyR that is necessary for CICR. Electron micrographs have shown protein bridges or "feet" that span the gap of ~12 nm between the SR and the T -tubules / sarcolemma. These feet, which could fill an area of ~30 nm x 30 nm, have been identified as the cytosolic portion of RyR (Anderson et al., 1989; Franzini-Armstrong et al., 1999; Inui et al., 1987). The association of the RyR with the DHPR creates a restricted diffusional compartment, known as the "fuzzy" space (Niggli and Lederer,

1990). This functionally restricted area enables small ionic fluxes to create the large local gradients necessary for E-C coupling, while still allowing Ca^{2+} to reach the contractile elements.

Recent studies have supported the existence of a highly organized sarcolemmal / T-tubular membrane; however, the molecular anatomy of the 'fuzzy' space or microdomain remains unclear. Numerous immunofluorescence and immuno-electron microscopy studies have shown that the DHPR and the RyR channels are colocalized along the apposed membrane surfaces of the T-tubule and the SR. Furthermore, Na^+/Ca^{2+} exchangers (NCX), voltage-gated Na^+ and K^+ channels and Na^+/K^+ pumps are also present in distinct domains within the sarcolemma and T-tubules indicating that some or all them may be localized within the 'fuzzy' space (Scriven et al., 2000; Scriven et al., 2002; Sedarat et al., 2000).

There are four major pathways involved in lowering $[Ca^{2+}]_i$ to levels sufficient to allow Ca^{2+} to dissociate from site II of troponin C and induce mechanical relaxation. In rabbit cardiomyocytes SERCA2a and NCX are the primary pathways, removing 70% and 28% of the activator Ca^{2+} respectively. The remaining 2% is removed by the sarcolemmal Ca^{2+}-ATPase (PMCA) and the mitochondrial Ca^{2+} uniport, and thus are known as the slow removal systems. Although, these two systems are not important on a beat-to-beat basis, recent studies have suggested that changes in the cytoplasmic $[NADH]/[NAD^+]$, which mirror changes in the mitochondria, could provide a point of feedback control for SR Ca^{2+} release (Bers, 2001; Bers, 2002; Cherednichenko et al., 2004; Meissner, 2004).

1.2.3 Excitation-Contraction Coupling in the Adult Myocardium

The described mechanism for E-C coupling in adult ventricular myocytes is calcium-induced-calcium release (CICR). The hypothesis that transsarcolemmal Ca^{2+} influx does not directly activate the myofilaments but instead triggers the release of Ca^{2+} from the SR that activates myofilaments was first demonstrated by Fabiato et el (Fabiato, 1983). Using skinned cardiac cells from a variety of mammalian and avian species, the investigators were unable to elicit myofilament contraction with simulated transsarcolemmal Ca^{2+} influx without first triggering SR Ca^{2+} release. When they compared the effects of stepwise increases in cytosolic [Ca^{2+}] before and after destruction of the SR, they found that the same increases in [free Ca^{2+}] that elicited contraction prior to destruction were unable to cause contraction in the myocytes with non-functional SR. Application of a higher [free Ca^{2+}] eventually led to contraction in these cells; however, it developed at a much slower rate. Additionally, it was demonstrated that SR Ca^{2+} release was not an all-or-none phenomenon that simply required the presence of Ca^{2+} to be activated, but was a graded response, which was dependent on both the concentration of transsarcolemmal Ca^{2+} as well as the rate of its delivery to the SR (Fabiato, 1983).

Numerous studies examining CICR in adult ventricular myocytes have established the importance of Ca^{2+} entry as the trigger, DHPR as the conduit through which it enters the cell and RyR as the SR Ca^{2+} release channel (Bers, 1991; Bers et al., 1990; Horackova, 1986; Langer, 1987; Nabauer et al., 1989; Pierce et al., 1987; Valdeolmillos et al., 1989; Wier et al., 1988). Nabauer et al., used rapid exchange (20 to 50 milliseconds) of the extracellular solutions surrounding intact ventricular myocytes, in which the intracellular calcium transients were measured, to demonstrate that the removal

of extracellular Ca^{2+} abolished the Ca^{2+} transient (Nabauer et al., 1989). Voltage-clamp studies showed that the magnitudes of the Ca^{2+} transients and cell contraction were proportional to the magnitude of the current through DHPR (I_{Ca}) initiated by the same test steps (Ferrier and Howlett, 2001). Additionally, contraction is suppressed by inhibiting I_{Ca} with the application of 15 μM nifedipine, a dihydropyridine that prevents the opening of DHPR (Pierce et al., 1987). Niggli et al examined the effects of membrane potential on Ca^{2+} release from the SR using caged Ca^{2+} (Niggli and Lederer, 1990). They found the intra-membrane charge movement did not affect SR Ca^{2+} release; it was dependent on the elevation of triggering Ca^{2+}. A similar study by Valdeolmillos et al, showed that the release of caged Ca^{2+} by UV light induced contraction, but when SR Ca^{2+} release was blocked by the application of ryanodine, the release of caged Ca^{2+} did not illicit a contraction, highlighting that a functional interaction between DHPR and RyR is necessary for CICR (Valdeolmillos et al., 1989).

CICR is an inherent positive feedback loop, producing it own trigger signal as the output signal, creating a paradox of control (Stern, 1992). One would expect that the Ca^{2+} released from the SR would activate nearby RyR receptors, eliciting a release of SR Ca^{2+} greater in magnitude then the originally triggered release. However, this explosive regenerative process is not observed under physiological conditions, instead SR Ca^{2+} release is tightly coupled to the amplitude of I_{Ca} (Ferrier and Howlett, 2001; Nabauer et al., 1989; Niggli and Lederer, 1990; Pierce et al., 1987). Early mechanistic models could not replicate the precise control exhibited in vivo. One reason for the conflict between the theoretical models of CICR and experimental evidence was due to the assumption that transsarcolemmal Ca^{2+} and SR Ca^{2+} are both released into the same cytosolic pool

(common-pool model) and that cytosolic [Ca^{2+}] rises and falls uniformly (Wang et al., 2004). However, if the trigger Ca^{2+} was separated from the Ca^{2+} released by the SR, as modelled by Wong et al, the positive feedback loop would be broken (Wong et al., 1987). The Wong model contained an 'appositional space" which could communicate freely with the SR and the plasma membrane, whereas the contractile elements were in a 'cytosolic space' which received Ca^{2+} from only the SR (Wong et al., 1987). The existence of a separate cytosolic space was also postulated by Lederer et al to explain experimental evidence demonstrating the ability of NCX to initiate CICR in the absence of I_{Ca} (Leblanc and Hume, 1990; Lederer et al., 1990; Niggli and Lederer, 1990; Stern, 1992). These researchers hypothesized ions transported through the DHPR, RyR, NCX, and Na^{+} channels would be accessible to the "fuzzy space". In addition, the space must restrict the rate of diffusion of ions, while still enabling equilibrium with the cytosol to be achieved (Lederer et al., 1990).

The concept of a functionally restricted intracellular space is fundamental to the local control model of CICR, which unified the experimental evidence with the theoretical speculation of a restricted space. Local control theory is critical to cardiac function as it provides a mechanism by which the positive feedback loop inherent in CICR could be broken; by separating the Ca^{2+} released from the SR and the Ca^{2+} that is the trigger controlling SR Ca^{2+} release. As presented by Stern (Stern, 1992), local control hypothesized that Ca^{2+} passing through DHPR would have privileged access to RyR on the SR membrane. Two mechanisms, voltage dependent inactivation via repolarization of the membrane and Ca^{2+}-dependent inactivation, would terminate I_{Ca} whereas the calcium sensitivity of RyR would be less than the ambient cytosolic calcium level,

preventing regenerative calcium release. Each RyR channel would sense the Ca^{2+} released by itself creating a feedback for Ca^{2+}-dependent inactivation. In this model, maximum amplification of the calcium signal would be dependent on the ratio between RyR and DHPR. To account for the high gain seen in CICR, Stern proposed that multiple RyR channels were clustered together and were able to sense the Ca^{2+} released from each other. Each cluster of RyR channels would be coupled to one DHPR channel, forming a calcium release unit (CRU), capable of local Ca^{2+} release events. The successive recruitment of CRUs controlled the graded response of CICR, at the whole cell level (Bers, 2001; Stern, 1992; Williams, 1997).

Local control, which mathematically could simulate the graded response of CICR, was given credence by the discovery of Ca^{2+} sparks. Sparks are small, spontaneous, non-propagating increases in $[Ca^{2+}]_i$ occurring in spatially restricted regions of quiescent cells. Sparks are believed to be the elementary release event in local control, as they are the result of the opening and closing of RyR clusters. Combining confocal microscopy with voltage-clamp protocols, Cannell et al, revealed that early termination of the triggering I_{Ca} resulted in a smaller Ca^{2+} transient, which was spatially non-uniform (Cannell et al., 1995; Cheng et al., 1993). As the duration of the triggering Ca^{2+} was increased, the spatially averaged $[Ca^{2+}]_i$ and the rate of rise increased, indicating that discrete release sites are activated by local I_{Ca}. These local release events were evoked over a range of potentials and shared many properties with sparks, including kinetics, amplitude, and spatial size indicating they both arise from the gating of a CRU. Once a CRU is activated, it is no longer dependent on trigger Ca^{2+} but on the intrinsic gating properties

of RyR. Termination would occur due to the spontaneous closing of a CRU, enabling a local decrease in $[Ca^{2+}]_i$ (Cannell et al., 1995).

E-C coupling via CICR is a multifaceted mechanism with complex activation and inactivation pathways that are precisely regulated. In the adult heart, the pathway of activation is clear; however, the termination pathway is poorly understood. The local control theory combined with the presence of Ca^{2+} microdomains is able to reconcile the experimental evidence with some of the theoretical challenges of CICR. The discovery of calcium sparks along with increasing information regarding the molecular architecture of cellular microdomains, appeared to have resolved the major paradox of CICR. In reality, the paradox has simply been transferred from a macroscopic level regarding control to a microscopic paradox of termination. Possible termination pathways exist, including local Ca^{2+} depletion, stochastic attrition, RyR inactivation and DHPR inactivation, although the latter is likely of less importance. Monte Carlo simulations of E-C coupling, which used inactivation properties of RyR that have been demonstrated in planar lipid bilayers, are unable to reproduce the stability and robustness of CICR. Only those models that increase the discrepancy between assumed and demonstrated RyR inactivation properties are able to recreate CICR with a terminating mechanism. CRUs ultimately remain regenerative in nature. Further research into the structure and function of RyR will provide additional information regarding the termination of CICR.

1.3 Functional Differences between Neonate and Adult Myocytes: an Overview

Early morphological studies have highlighted the striking differences between neonatal and adult cardiac myocytes, differences that suggest a much greater dependence on transsarcolemmal Ca^{2+} flux during E-C coupling in the neonate. Neonatal myocytes are significantly smaller in size and lack a T-tubule system (Artman et al., 2000; Hoerter et al., 1981). The smaller cell size contributes to a larger surface-to-volume ratio that remains steady until 8-15 days (species dependent) post-partum, at which time the ratio begins to decrease steadily toward adult values. The decrease occurs despite the appearance of the T-tubular system, around 10 days post-partum in the rabbit, which contributes significantly to total surface area (Hoerter et al., 1981). In addition, the SR appears to be less well developed and the RyR is not functionally coupled to DHPR (Callewaert, 1992; Cannell et al., 1995; Fozzard, 1991; Sedarat et al., 2000; Williams, 1997). It has recently been shown that the SR present in neonate myocytes is functional and has Ca^{2+} loads that are at least comparable in magnitude to their adult counterparts. However, neonate myocytes exhibited smaller fractional SR Ca^{2+} release during steady state contraction and inhibition of SR Ca^{2+} release did not lessen contraction to the same degree as that seen in adult myocytes. These results underscore the diminished importance of SR Ca^{2+} release in E-C coupling of immature hearts (Balaguru et al., 1997; Haddock et al., 1999).

The dependence on transsarcolemmal Ca^{2+} flux for contraction has been demonstrated through functional studies comparing differences in tension development, recovery from 0 mM Ca^{2+}, and differences in Ca^{2+} flux between neonate and adult myocytes (Chin et al., 1990; Haddock et al., 1999; Klitzner and Friedman, 1988).

Klitzner et al (Klitzner and Friedman, 1988) looked at tension development in response to depolarization, which mimicked an action potential. Adult myocytes displayed biphasic tension development, peaking early and then relaxing to a steady-state level. Peak tension occurred after the repolarization phase of the action potential. This is in contrast to the neonate, in which tension increased monotonically, peaking at the end of the depolarization phase of the action potential and decreasing immediately upon repolarization. The biphasic nature of tension development present in the adult is consistent with Ca^{2+} being released from the SR in a CICR manner. The degree of biphasic tension development increases with age, corresponding to increased importance of SR Ca^{2+} release. This decrease in importance of SR Ca^{2+} release was corroborated by studies looking at the recovery of contraction amplitude after perfusion with 0 mM Ca^{2+} (Chin et al., 1990).

Under normal conditions, one observes spontaneous release of SR Ca^{2+} via leakage from membrane channels, as well as passive diffusion, which is returned to the SR via SERCA2a. When myocytes are perfused with 0 mM Ca^{2+}, the Ca^{2+} lost from the SR is preferentially removed from the cytosol via the NCX, reducing SR Ca^{2+} levels. Thus, adult myocytes are unable to regain full contraction amplitude until the SR is reloaded. Chin et al (Chin et al., 1990), demonstrated that when neonatal myocytes are perfused with 0 mM Ca^{2+} for either 1 or 5 minutes, they require fewer beats to return to control levels after reperfusion with 0.1 mM Ca^{2+} than their adult counterparts. As well, the initial beat after reperfusion was 85% of the control in the neonate, and only 20% in the adult. Adult myocytes require more beats to recover from perfusion with 0 mM Ca^{2+}, and have significantly decreased contraction amplitude in the initial beat upon

reperfusion with 0.1 mM Ca^{2+} (Chin et al., 1990). These studies demonstrate that there is greater dependence of contraction on SR Ca^{2+} release in adult in comparison to neonate myocytes.

If cytosolic Ca^{2+} buffering capacity was the same in both neonatal and adult myocytes, the increased dependence on transsarcolemmal Ca^{2+} flux in the neonate would lead to the expectation of increased expression levels and current density of DHPR in neonatal myocytes, the main route of Ca^{2+} influx. However, Ca^{2+} buffering is reported to be 2-3 times lower in neonatal ventricular myocytes, therefore, if expression levels and current density of DHPR remained constant, I_{Ca} would have a greater affect on myofilament activation in the neonate (Bassani et al., 1998). In contradiction to the increased importance of transsarcolemmal Ca^{2+} influx, neonatal myocytes exhibit a decreased DHPR current density and mRNA levels (Chin et al., 1990; Huynh et al., 1992; Klitzner and Friedman, 1988; Klitzner et al., 1991; Qu and Boutjdir, 2001; Wetzel et al., 1991; Wetzel et al., 1993). As shown by Huynh et al., and others, the current density of DHPR is significantly smaller in neonatal myocytes compared to the adult myocyte. The decrease in current density is greater than would be expected due to differences in membrane capacitance, a measure of cell surface area. A 1.7-10 fold difference between neonate and adult myocytes DHRP current density has been reported (Huynh et al., 1992; Tibbits et al., 2002; Wetzel et al., 1991; Wetzel et al., 1993). Furthermore, inhibition of DHPR does not significantly decrease peak tension development in neonate myocytes, suggesting that the rise in intracellular Ca^{2+} attributable to DHPR channels is smaller in the neonate than in adult myocytes (Wetzel et al., 1995). The dramatic increase in I_{Ca} occurring postnatally suggests that during development an alternative Ca^{2+} pathway may

be functioning to bring additional Ca^{2+} into the cell to induce contraction with or without CICR.

It has been proposed that NCX may contribute to Ca^{2+} influx via reverse mode activation during E-C coupling in the neonate heart. NCX expression is dramatically up regulated during fetal and neonatal periods and declines postnatally, as reflected in current density, western blot and northern blot analyses; these factors all enhance the ability of NCX to transport Ca^{2+} across the SL in the neonate (Artman, 1992; Artman et al., 1995; Koban et al., 1998; Qu and Boutjdir, 2001; Qu et al., 2000). It has been demonstrated in neonate myocytes that NCX operating in reverse mode provides a significant portion of the Ca^{2+} regulating cell contraction, and that I_{NCX} is responsible for peak contraction (Wetzel et al., 1995).

At rest, NCX operates in normal mode, extruding Ca^{2+} and bringing Na^+ into the cell with a stoichiometry of 1:3, creating a net inward current, I_{NCX} with a reversal potential (E_{NCX}) equal to $3E_{Na} - 2E_{Ca}$ (Bers, 2001). The electrogenic nature of NCX gives rise to the dependency of the direction and amplitude of I_{NCX} on the internal and external $[Na^+]$ and $[Ca^{2+}]$ as well the membrane potential (E_m) of the cell. Reverse mode NCX, resulting in Ca^{2+} influx, is thus initiated when the membrane potential (E_m) is less then E_{NCX} which is triggered by: increasing $[Na^+]_i$, decreasing $[Ca^{2+}]_i$ to alter E_{NCX} or by lowering E_m by membrane depolarization. During excitation, fast inactivating Na^+ channels open allow an influx of Na^+ ions to increase the subsarcolemmal $[Na^+]_i$ and drive the membrane potential towards ~ 20 mV. These conditions favour reverse mode NCX, however, depolarization of the membrane also leads to the opening of DHPR channels, creating an influx of Ca^{2+}, which would inhibit NCX reverse mode. Therefore,

to enable NCX reverse mode to bring in enough Ca^{2+} to trigger contraction, either through Ca^{2+} influx directly or via CICR, NCX would need to be preferentially located in a microdomain so that it may sense a local rise in $[Na^+]_i$ sufficient to induce reverse mode and / or NCX would need to be coupled to RyR so that I_{NCX} may trigger CICR (Bers et al., 1990; Feron and Kelly, 2002; Johnson et al., 1991; Leblanc and Hume, 1990; Levesque et al., 1991; Weber et al., 2003).

Immunofluorescence studies have indicated that in the adult myocyte, NCX is localized along the plasma membrane and the T-tubules in distinct domains (Chen et al., 1995; Kieval et al., 1992; Scriven et al., 2000). However, in developing myocytes, two published reports suggest NCX to be homogenously distributed along the plasma membrane (Chen et al., 1995; Haddock et al., 1999). A homogenous distribution of NCX in neonate myocytes is unlikely to favour Ca^{2+} influx by NCX reverse mode activity. The global rise in $[Na^+]_i$ that occurs due to I_{Na} during an action potential is very small and is likely incapable of inducing reverse mode operation of NCX (Weber et al., 2003). Yet functional studies on neonate myocytes have demonstrated that I_{NCX} provides a significant portion of the Ca^{2+} regulating cell contraction (Wetzel et al., 1995). We, therefore, hypothesize that NCX is not homogenously distributed in neonate myocytes and that some or all are localized within sarcolemmal microdomains (e.g. caveolae). The localization of NCX in a microdomain would enable local ion concentrations to accumulate in favour of reverse mode operation that is sufficient to initiate CICR. Furthermore, we suggest that in ventricular neonate myocytes, these caveolar microdomains form a structural relationship with the SR as seen in arterial vascular smooth muscle cells (Lohn et al., 2000).

1.4 Structure and Properties of NCX

The NCX is an integral membrane protein found in all tissue types. It is a rapid responding, high capacity Ca^{2+} transport system that is essential in maintaining calcium homeostasis in variety of tissues. NCX is a secondary active transporter with the net direction of Ca^{2+} transport dependent on both the electrochemical gradients for Na^{+} and Ca^{2+} and membrane potential (Philipson and Nicoll, 2000). Although NCX is found in almost all tissue types, its importance is dependent upon its abundance and the number of alternate Ca^{2+} transport systems that are present in the tissue; hence, it appears to be of relatively low importance in the liver, but plays a major regulatory role in smooth muscle, kidney, brain and cardiac cells. NCX is most important in cardiac cells, where its primary responsibility is calcium extrusion during the E-C coupling cycle (Hilgemann, 2004; Philipson and Nicoll, 2000; Shigekawa and Iwamoto, 2001).

NCX belongs to a superfamily of cation/Ca^{2+} exchangers that is defined by the presence of highly conserved α repeats in two clusters of hydrophobic regions separated by a hydrophilic loop, rich in acidic residues (Schwarz and Benzer, 1997). This superfamily is composed of five smaller families, YRBG, CAX (H^{+}/Ca^{2+} exchangers), CCX (cation/Ca^{2+} exchanger), NCKX (K^{+} dependent NCX) and NCX (K^{+}-independent NCX) (Cai and Lytton, 2004; Philipson and Nicoll, 2000). In mammals, NCX is a multigene family of three genes NCX1, NCX2 and NCX3. It is believed that all three isoforms have a very similar molecular structure, as they share an amino acid sequence that is highly conserved. After the exclusion of leader peptides and potential alternative splice sites, the percent amino acid identity is 68% between NCX1 and NCX2, 73% between NCX1 and NCX3, and 75% between NCX2 and NCX3. NCX2 and NCX3 are

primarily expressed in the brain and skeletal muscle, whereas NCX1 is ubiquitous but is most highly expressed in cardiac tissue. Another unique characteristic of NCX1 is the presence of an alternative splicing region in the cytoplasmic loop, absent in both NCX2 and NCX3, which gives rise to a number of splice variants (at least ten) including the cardiac isoform NCX1.1 (Li et al., 1994; Nicoll et al., 1990; Nicoll et al., 1996; Philipson and Nicoll, 2000).

The cardiac sarcolemmal NCX was the first isoform to be isolated and subsequently cloned (Hryshko et al., 1993; Nicoll et al., 1990). From the original cloning, it was predicted that NCX1.1 was comprised of 970 amino acids and had a deduced molecular weight of 110 kDa. In actuality, the native exchanger is 938 amino acids; this discrepancy is the result of post-translational modifications, which include the cleavage of a signal peptide (Hryshko et al., 1993). On immunoblots, antibodies to NCX react with exchanger polypeptides of 160, 120 and 70 kDa. It is generally believed that the 70 kDa band is a proteolytic fragment, while the faint 160 band is due to intact disulfide bonds (McDonough et al., 2002; Nicoll et al., 1990; Nicoll et al., 1999; Philipson and Nicoll, 2000).

The exchanger was originally modelled to have 12 transmembrane segments (TMS), with a large (>500 a.a.) intracellular loop between TMS 6 and 7 (Nicoll et al., 1990). It is now generally accepted that NCX has 9 TMS, with a larger intracellular loop (550 amino acids) between TM 5 and 6 (Figure 3). This large hydrophilic region is not essential for ion translocation, as demonstrated by deletion mutagenesis, but is highly important in the regulation of NCX (Matsuoka et al., 1993). It contains the XIP (e**X**changer **I**nhibitory **P**eptide) site, the Ca^{2+} binding domains, the alternative splicing

region, as well as the β repeats (β-1 and β-2), which are regions of about 60 amino acids that have a high degree of similarity. The functional importance of these repeats is not yet known. The N-terminal and C-terminal ends of the TM domains contain the α repeats (α-1 and α-2), these regions of identity are 40 amino acids in length and are highly conserved within the NCX gene family and other cation exchangers throughout evolution (Cai and Lytton, 2004; Cook et al., 1998; Iwamoto et al., 1999; Philipson and Nicoll, 2000; Schwarz and Benzer, 1997; Shigekawa and Iwamoto, 2001). As discussed below, several key features of these regions indicate they play a major role in ion translocation.

The functional importance of the α-repeat regions is implied by the conservation of its sequence throughout evolution. This assumption is supported by both phylogenetic and functional analyses. Each of the two α-repeat contain the acidic residues D and E at positions 65 and 246, respectively, which are absolutely conserved. The role of these residues in ion translocation could be to assist in overcoming the energy barriers to ion translocation by neutralizing the two positive charges on Ca^{2+}. Included in the α - repeats are other acidic amino acids including seronine, theronine, and asparagine, which could assist in the binding and transportation of Ca^{2+}. In addition, the α-repeat regions are enriched in glycine and alanine, which may allow for structural flexibility. Furthermore, two glycines, one in each region, are absolutely conserved (Cai and Lytton, 2004; Marshall et al., 2005). The importance of the α-repeat regions has also been demonstrated using site-directed mutagenesis. In general mutations in the α-repeat regions have resulted in a non-functional exchanger, even with conservative substitutions (e.g. S110A) (Nicoll et al., 1996).

1.5 Structure and Properties of RyR

The release of Ca^{2+} from intracellular stores to amplify external signals that modulate intracellular signalling events occurs in almost all cell types. There are two families of channels responsible for providing the pathway of regulated release from these internal stores, RyR and **I**nositol tri**P**hosphate **R**eceptors (IP_3R). These proteins, which belong to separate gene families, are often referred to as Ca^{2+} release channels and share a significant degree of homology. In cardiac myocytes, RyR is found on the membrane of the SR and is responsible for SR Ca^{2+} release in response to the extracellular Ca^{2+} flux from DHPR. The efficiency of communication between DHPR and RyR is a factor in determining the amount of Ca^{2+} released, and the subsequent strength of myocyte contraction (Benkusky et al., 2004; Marks, 2001; Williams et al., 2001).

Currently, three isoforms of RyR, all encoded by separate genes, have been cloned and sequenced: RyR1, RyR2 and RyR3. Amino acid comparisons of the isoforms show a high degree of amino acid identity between RyR3 / RyR2, RyR3 / RyR1, and RyR1 / RyR2: 70%, 67% and 67% identity, respectively. RyR1 is expressed predominately in skeletal muscle and is therefore commonly referred to as the skeletal muscle isoform. The highest expression levels of RyR2 are in cardiac muscle while that of RyR3 are in the brain, and thus are referred to as the cardiac and brain isoforms, respectively. Interestingly, RyR2 and RyR3 share the highest degree of identity and RyR2 is relatively abundant in the cerebellum, where RyR3 levels are low. RyR3 is expressed in some cardiac tissues such as the Purkinje fibres, specialized conductive myocardial fibres (Berne et al., 1998; Hakamata et al., 1992; Nakai et al., 1990). All

three RyR isoforms have similar Kite-Dolittle hydropathicity profiles, predicting four highly hydrophobic segments, M1-M4, in the carboxy terminal with the remaining region being hydrophilic. The M3 and M4 segments are highly conserved in all ryanodine receptors, as are four repeated sequences occurring in two tandem pairs, and this may be indicative of functional importance (Hakamata et al., 1992; Nakai et al., 1990; Takeshima et al., 1989). Although numerous secondary structures have been predicted, a universally agreed upon structure has not yet been deduced.

Native RyR2 was first isolated and purified to homogeneity in 1987 by Inui et al. Electron microscopy of the purified receptor demonstrated that it existed as a quatrefoil or four-leaf clover structure (with four-fold symmetry) that was similar to the "foot" structures of the SR (Anderson et al., 1989; Inui et al., 1987). It is the largest known membrane protein with a total molecular mass of 2.3 x 10^3 kDa. The channel is now known to be a homotetramer with the individual monomers having a molecular weight of 565 kDa. RyR2 has both high and low affinity binding sites for the plant alkaloid ryanodine, which bind with a 4-5 fold higher binding affinity than in RyR1 (Anderson et al., 1989; Inui et al., 1987; Meissner et al., 1988; Williams et al., 2001). Analysis of the amino acid sequence has shown several consensus ligand binding sites, which may be potential modulators (eg ATP, caffeine, and calmodulin) (Fill and Copello, 2002). When expressed in planar lipid bilayers, RyR has a conductance of 70 pS in the presence of 50 mM Ca^{2+}. This conductance is sensitive to a number of cytosolic factors, including Ca^{2+}, ATP, Mg^{2+}, and H^+ (Inui et al., 1987; Meissner et al., 1988; Nakai et al., 1990). Additionally, RyR open probability can be modulated by protein-protein interactions including interactions with FK-506 binding proteins (FKBP12), calmodulin, and sorcin

(Benkusky et al., 2004; Bers, 2004; Jayaraman et al., 1992; Mayrleitner et al., 1994; Timerman et al., 1994; Williams et al., 2001).

The 3-D structure of RyR, based on cryoelectron tomography, has been described as being similar to that of a mushroom with the cytoplasmic N-terminus domain forming the "cap" and the "stalk" being formed by the C-terminus membrane-spanning segments (Williams et al., 2001). Surface representations show two main structural components, the cytoplasmic component has the shape of a large square prism, occupying an area 29 x 29 x 12 nm in dimension. A smaller protruding mass is attached to one of the prism's faces and is thought to be the membrane spanning component and contains the putative Ca^{2+} conducting pathway (Radermacher et al., 1994). Analysis of the primary amino acid sequence along with recent mutagenesis experiments suggest that the transmembrane domains are in the C-terminus and are able to form a functional channel, whereas the N-terminus contains many of the regulatory sites (Ma et al., 2004). The membrane topology of RyR remains elusive; however, different models have been proposed which predict between 4-12 transmembrane segments. Several studies have provided evidence that both the NH_2 and COOH termini are located in the cytoplasm, requiring an even number (four to ten) of transmembrane segments with an ion selectivity filter present within a region residing between the last two segments, similar to potassium channels (Grunwald and Meissner, 1995; Ma et al., 2004; Shah and Sowdhamini, 2001; Takeshima et al., 1989; Tunwell et al., 1996). Figure 4 shows a putative topology of cardiac RyR as the original 4 TM model, along with a visual summary of the current modifications made based on recent findings.

1.6 Confocal Microscopy and Deconvolution: an Overview

1.6.1 Confocal Microscopy

The laser scanning confocal microscope (LSCM) has been a major advancement in optical microscopy. LSCM offers many advantages over conventional microscopy in that it allows a controllable depth of field, reduction of out-of-focus light, and the ability to collect optical sections from thick specimens (up to 100 μm) allowing the visualization of complex three dimensional structures. Although other forms of microscopy can image in three dimensions, LSCM does so intrinsically. This has enabled researchers to analyze the location of proteins with respect to one another and with respect to the cellular architecture (Hibbs, 2000).

The main advantage of LSCM is its ability to limit the depth of field by reducing contributions out-of-focus light by using an aperture / pinhole device in front of the point detector(s) (Figure 5). Much of the optical pathway of a confocal microscope is similar to a conventional epi-fluorescence microscope. In conventional epi-fluorescence, the entire sample is illuminated and a "real" image is produced that is observable by eye. However, because the entire sample is illuminated there are significant contributions of light from out-of-focus planes, reducing resolution of all "non-thin" samples. LCSM is different in that it uses a laser as the excitation source rather then a conventional arc lamp. Light coming from a laser is highly collimated and is more readily able to form what is commonly referred to as a diffraction-limited excitation spot. This excitation spot is "scanned" over the sample in a raster pattern to produce the image. Unfortunately, the excitation spot is shaped more like an hourglass than it shaped like an actual spot (see Figures 7 and 8). A significant amount of excitation energy is found above and below the

focal plane and thus there is also significant amount of light emission from these planes. To minimize non-focal plane contributions, a confocal (same-focus) aperture is placed at a conjugate image plane, hence the name **L**aser (excitation source) **S**canning (scanning of the diffraction limited spot) **C**onfocal (the use of a confocal aperture to reduce out-of-focus emission) **M**icroscope. The placement of the source pinhole in front of the light source (i.e. laser) controls the size of the illuminating light cone to a diffraction-limited spot (Airy disk) point on the specimen. Excited spots emit light as point sources which have an Airy disk size that is inversely proportional to the numerical aperture of the objective and the wavelength (λ) of the excitation beam. Therefore, the diameter of the detector pinhole must be equal to the diameter of the central spot of the Airy disk to allow all the light originating from the focus plane to reach the detector (Pawley, 1995). With only a single point illuminated, the illumination intensity rapidly falls off above and below the plane of focus as the beam converges and diverges, thus reducing excitation of fluorescence from interfering objects situated outside of the focal plane being examined. The excitation light behaves as a point source so the illumination intensity rapidly falls off above and below the plane of focus reducing the efficiency of excitation of fluorophores from these planes. Therefore, having the correct diameter of the detector pinhole is critical to reducing the amount of out-focus light that is able to reach the detector (Hibbs, 2000; Pawley, 1995).

In addition to out-of-focus light, image degradation occurs due to components within the imaging system. This degradation can be measured by examining the distortion of objects of known dimensions such as subresolution fluorescent beads and determining the point spread function (PSF). The PSF is a measure of convolution;

distortion occurring due to the combined effects of all optics and filters in the beam path. If the convolution is known, then theoretically it can be reversed through the application of mathematical algorithms, a process known as deconvolution (Hibbs, 2000; Pawley, 1995).

The optical path of the LSCM is set to focus light to a specific point in the plane of focus. To create a 2-D image, the focal spot is scanned across the sample and the fluorescent signal collected at each point is recorded, digitized and displayed on a screen with the appropriate digital intensity values and XY co-ordinates. Since the displayed image is produced primarily from signal originating from a single plane within the specimen, it has been termed an optical slice. A 3-D image of a specimen is created by collecting images of optical slices from adjacent focus planes and integrating them with image processing software (Cox, 2002; Hibbs, 2000; Pawley, 1995) .

1.6.2 Deconvolution

Deconvolution is a mathematical method to undo degradations introduced by the imaging process, described by convolution. Depending on the type of algorithm used, deconvolution will either re-assign or remove out-of-focus light, resulting in an image which appears sharper with higher contrast (Landmann, 2002; Larson, 2002; Malkusch et al., 2001; McNally et al., 1999; Wallace et al., 2001). Deblurring algorithms, such as Nearest Neighbour, are 2-D deconvolution algorithms that subtract blur using a plane-by-plane analysis. These types of algorithms are fast and computationally economical. However, because signal is being removed instead of being reassigned, the total signal contained in the image is reduced, decreasing the signal-to-noise ratio (SNR). In addition, the plane-by-plane analysis adds together the noise from adjacent planes further

degrading the SNR. 3-D deconvolution algorithms use information from all focal planes simultaneously to re-assign out-of-focus light. The simplest models were based on Fourier transformations of the frequency components. However, these models of image acquisition and recording were not reliable approximations of the actual process of image formation, a necessity for deconvolution (Landmann, 2002; McNally et al., 1999; Wallace et al., 2001).

Maximum Likelihood Estimation (MLE) takes into consideration the random behaviour of light (Poisson distribution) and noise (Gaussian distribution), viewing deconvolution as a statistical estimation problem as opposed to modelling how image acquisition and recording occur. Very simply, MLE finds the parameters that make the observed data most likely. Using constrained iterative algorithms; a first approximation is made of the true image and convolved with the PSF, resulting in blurred estimates of the image. The blurred estimates are compared to the recorded image; the difference between the blurred estimate and the recorded image is measured, this error is used to make a new blurred estimate, which is compared to the recorded image. This iterative process continues until the difference between the blurred estimate and the recorded image reaches a minimum.

1.6.3 Colocalization

The ability to focus into specific planes of the cell has contributed significantly to research on protein-protein interactions. In conventional immunofluorescence, antibodies specific to different proteins can be (or normally are) conjugated to fluorophores with different excitation and emission wavelengths. Traditionally these antibodies would be used to stain cells and the distribution of the proteins within the cells could be elucidated

only in 2-D space. The ability to create 3-D images and optical slices has enabled researchers to determine if proteins that lie adjacent to one other in the X-Y plane, belong to the same optical slice. The assertion of two proteins next to one another in the X-Y as well as the same optical slice (Z plane) has allowed the colocalization of two proteins in a given 3-D space to be established (Hibbs, 2000; Pawley, 1995).

The term colocalization is defined as the spatial arrangement of two structures or components in which they occupy the same defined 3-D space (e.g. 100nm x 100 nm x 250 nm voxel). As most biological proteins are subresolution, the term reflects the presence of the fluorescent signal from both probes. Using different fluorescent probes to label structures and collecting the emission spectra into separate channels, the colocalization of multiple structures can be studied. A colocalized image is formed by overlaying the image from one channel over the image collected by the second channel. The regions of overlap between the fluorescent probes are then analyzed to determine the degree of colocalization (Landmann, 2002; Sedarat et al., 2004).

Colocalization studies using LSCM are extremely useful as they enable the researcher to visualize the distribution of proteins in vivo. However, analysis of colocalization through LSCM can be affected by many factors, which can alter the validity of the results. In addition to the factors associated with microscopy in general, laser misalignment, chromatic aberrations, bleed through, and noisy images can lead to false positives. Therefore, it is important to take the necessary steps to minimize these factors (i.e. dual channel collection, appropriate filter selections and correct pinhole size) (Hibbs, 2000; Landmann, 2002; Sedarat et al., 2004).

Whether or not two fluorescent signals overlap in 3-D space is a matter of resolution. In the extreme case, it is obvious that two structures cannot occupy exactly the same location even though it may appear so when observed from a microscope with low resolving power. Consequently, the degree of colocalization will depend on the resolving power of the microscope (Cox and Sheppard, 2004; Hibbs, 2000; Paddock, 1999; Pawley, 1995; Schrader et al., 1996). Images obtained using LSCM can be optimized to have a higher resolution due to the ability to reduce out-of-focus light with a pinhole. Even after using deconvolution, the best confocal microscopes will only have a resolution of 100 nm in the lateral plane and substantially less in the axial plane (Cox and Sheppard, 2004; Hibbs, 2000). The **F**ull **W**idth **H**alf **M**aximum (FWHM) is the diameter of the Airy disk at which the intensity of the central spot drops to half its maximum and is frequently used as a measure of resolution. The Zeiss LSM 5 Pascal has a measured FWHM of 183 nm in the lateral axes. Accordingly, confocal microscopy may be able to demonstrate that proteins are contained within a range of possible separation distances, but it is not possible to establish if a functional relationship exists

1.7 Research Objectives and Hypotheses

1.7.1 Objectives

To provide insight into the mechanism of neonate ventricular myocyte excitation–contraction (E-C) coupling. To establish if a structural relationship exists between NCX and RyR, such that initiation of NCX reverse mode during E-C coupling may trigger SR Ca^{2+} release via RyR.

1.7.2 Hypotheses

1) NCX is not homogenously distributed on the plasma membrane of neonate myocytes prior to the development of the transverse tubule system
2) NCX is colocalized with RyR in the neonate myocyte and the degree of colocalization decreases with age

CHAPTER 2:
MATERIALS AND METHODOLOGY

2.1 Animals

Immature (3-, 6-, 10- and 20-day old) and adult (56-day old) New Zealand White rabbits of either sex were used for this study. For each age group 5 hearts and 10 cells / heart were studied for a total of 250 cells in 5 age groups.

2.2 Antibodies

The antibody to the Na^+/Ca^{2+} exchanger was an affinity purified monoclonal antibody R3F1, obtained from Swant Antibodies (0.7mg/mL, Bellinzona, Switzerland). The antigen used was purified canine cardiac Na^+/Ca^{2+} exchanger. This antibody recognizes two epitopes on neighbouring but non-overlapping sequences of the large (~550 a.a.) hydrophilic region of the exchanger which connects the putative transmembrane segments 5 and 6 and has been termed the F loop, which is modelled to be on the intracellular side of the plasma membrane.

Previously characterized monoclonal anti-RyR was obtained from Affinity Bioreagents (IgG_1, #MA3-916, 1 mg/mL, Golden, CO) and was developed in C3-33 cells using canine cardiac ryanodine receptor as an antigen (Sedarat, 1999). MA3-916 detects RyR2, but also weakly detects RyR1, in amphibian, canine, chicken, fish, guinea pig and rat tissues.

Secondary antibodies were donkey anti-goat conjugated to Alexa 488 and donkey anti-mouse conjugated to Alexa 555 from Molecular Probes (2 mg/mL, Eugene, OR). These antibodies were affinity-purified to minimize cross-reactivity. Since both primary antibodies were from the same host (mouse), the immunoglobins from the first primary antibody (mouse anti-RyR) needed to be sterically covered with a non-conjugated monovalent Fab fragment of a secondary antibody. Monovalent antibodies have only one antigen binding site, in contrast to whole IgG molecules and $F(ab')_2$ fragments of IgG which have two antigen binding sites. Therefore, after binding to its primary antibody, the monovalent fragment does not have any open binding sites with which to capture the second primary antibody preventing an overlap of labelling. Goat anti-mouse monovalent Fab fragment was used to mask the mouse anti-RyR antibody at a concentration of 200 μg/mL (Jackson ImmunoResearch, Westgrove, PA).

2.3 Western Blot Analysis of Antibody Specificity

2.3.1 Tissue Homogenization

A complete, mini, EDTA-free protease inhibitor tablet (Roche Applied Sciences, Laval, QC) was dissolved in 7 mL of homogenization buffer containing in (mM): 250 Sucrose and 20 TES (N-tris(hydroxymethyl)methyl-2-aminoethanesulfonic acid; 2-(2-[hydroxy-1,1-bis(hydroxymethyl)ethyl]amino)ethanesulfonic acid). Ventricles of hearts from 10-day old rabbits were quickly excised and placed in a volume of the homogenization buffer + inhibitor solution (1 mL buffer / 100 mg of wet weight). Ventricles were minced before being blended 2X at 20 rpm for 12 seconds (IKA Labortechnik, Staufen, Germany). Homogenized samples remained on ice and were subsequently centrifuged (Baxter Canlab Biofuge A) at 1300 x g for 5 minutes at 4°C.

The supernatant was transferred to clean Eppendorf tubes and stored at -80°C until further use. Total protein concentration of the supernatant was determined using the Bradford method (Bradford, 1976).

2.3.2 Gel Electrophoresis and Western Blotting

Calculated volumes of homogenate were added to Laemmli buffer containing: 60 mM Tris, 2% (w/v) sodium dodecyl sulphate (SDS), 10% (v/v) glycerol, and 5% (v/v) β-mercaptoethanol (pH 6.8), to adjust to a protein concentration of 70 μg / 35 μL volume. Membrane proteins were denatured by heating to 95°C for 4 minutes prior to loading into a 10% SDS polyacrylamide gel (60 μg protein / 30 μL volume loaded per lane) for separation via gel electrophoresis. Samples were run at 200 V and 150 mA at 4°C for approximately 60 minutes using an electrophoresis running apparatus immersed in buffer solution containing (in mM): 25 Tris, 125 glycine, and 0.1% (w/v) SDS (pH 8.3). Separated proteins were transferred onto an activated polyvinylidene difluoride (PVDF) membrane via a transfer apparatus immersed in cold transfer buffer containing (in mM): 25 Tris, 192 glycine, and 10% (v/v) methanol (added fresh) (pH 8.3). All transfers were done at 4°C at 30 V and 100 mA overnight. Transfer efficiency and protein loading was verified by staining membranes with Ponceau Red stain (Sigma), after rinsing in ddH_20. Membranes were washed with volumes of ddH_20 and TBST containing (in mM): 50 Tris, 159 NaCl, and 0.5% (v/v) Triton X-100 (pH 7.4), to remove Ponceau stain prior to immunodetection.

Non-specific binding sites were blocked with 5% BSA for 90 minutes at room temperature, under gentle agitation. Membranes were washed with TBST and incubated

overnight at 4°C with R3F1 anti-NCX (1:8000) in TBST containing 1% (w/v) BSA and 0.5% (w/v) NaN_3. After thorough washing procedures with TBST, membranes were exposed to goat anti-mouse IgG conjugated to horseradish peroxidase (HRP) for 90 minutes at room temperature (Santa Cruz Biotechnology Inc. Santa Cruz, CA). Secondary antibodies were prepared fresh in TBST containing 1% (w/v) BSA at a dilution of 1:10000. Membranes were washed with TBST, followed by TBS containing (in mM): 50 Tris and 150 NaCl (pH 7.4), before visualization on Hyperfilm (Amersham Biosciences, Piscataway, NJ) using enhanced chemiluminescence protocols (ECL) (Amersham Biosciences, Piscataway, NJ).

2.4 Immunocytochemical Analysis

2.4.1 Ventricular Myocyte Isolation

Ventricular myocytes were obtained by enzymatic dissociation as described by Huang et al (Huang et al., 2004). Briefly, rabbits were anticoagulated with Heparin (15 mg/kg body weight) and anesthetised with pentobarbital sodium (65 mg/kg body weight). Immature rabbits were injected intra-peritoneally, while mature rabbits were injected intravenously via cannulation of a vein in the ear. Hearts were rapidly excised and cooled in ice cold Ca^{2+}-free Tyrode's solution containing (in mM): 100 NaCl, 10 KCl, 1.2 KH_2PO_4, 5 $MgSO_4$, 50 taurine, 20 glucose, and 10 HEPES (pH 7.2), before being set up on a Langendorff apparatus and retrogradely perfused with 15 mL of Ca^{2+}-free Tyrode's solution to clear the coronary arteries and heart tissue of blood. After washing, the heart was digested by switching the perfustate to (1) Ca^{2+}-free Tyrode's solution containing collagenase (0.06-0.2 mg/mL, Yakult, Japan) and BSA (1 mg/mL, Sigma), and then (2) protease (0.05-0.1 mg/mL, Sigma) and BSA (1 mg/mL) dissolved in Storage

Solution containing (in mM): 120 $C_5H_8NO_4K$, 5 Mg_2Cl_2, 20 taurine, 1 EGTA, 10 glucose and 10 HEPES (pH 7.3). The flow rate, enzyme concentrations, and volumes were adjusted to account for age-related differences in rabbit heart composition (Table 1). All solutions were aerated with 100% oxygen and warmed to 37°C prior to perfusion. Following digestion, the ventricles were removed and minced in storage solution with an equal volume of 2% (w/v) paraformaldehyde to release and fix individual myocytes. The cell suspension was then filtered through a nylon mesh (200μm) to remove tissue chunks. Myocytes were fixed for 10 minutes, after which they were quenched for aldehyde groups in 100 mM glycine buffer (pH 7.4) for 10 min. Cells were subsequently permeabilized in phosphate buffered saline (PBS) containing in (mM): 2.7 KCl, 1.5 KH_2PO_4, 137 NaCl, and 8 $Na_2HPO_4{\cdot}7H_2O$ (pH 7.4) with 0.1% (v/v) Triton-X100 for 10 min. The permeabilization solution was removed with 3 x 10 min washes in PBS.

Table 1: Parameters for myocyte isolation

Age (day)	3	6	10	20	56
Collagenase concentration (mg/mL)	0.06	0.10	0.10	0.10–0.20	0.20
Collagenase volume (mL)	10	10	15	10-40	100-150
Protease concentration (mg/mL)	0.05	0.07	0.10	0.10	0.10
Protease volume (mL)	10	10	10	10-15	50
Perfusion speed (mL/min)	1.0	1.0	1.0	1.5	3.0-3.5

2.4.2 Indirect Immunofluorescence Labelling

Indirect immunocytochemistry was performed on fixed cells using the method of Moore (Bullock and Petrusz, 1982; Moore et al., 1993). Fixed myocytes were allowed to settle on pre-cut quartz coverslips (20 mm x 20 mm, 1.7 mm thick) that were made positively charged by coating with poly-L-lysine. The myocytes, after settling, were washed with PBS to remove excess fluid and double labelled with 100 μL of primary antibodies diluted in antibody buffer solution containing (in mM): 75 NaCl, 18 Na_3·citrate, 1% (w/v) BSA, 0.05% (v/v) Triton X-100, 0.02% (w/v) NaN_3 and 2% (v/v) goat serum (added fresh). Excess primary antibody was removed by washing the cells 3 x 5 minutes in antibody wash solution containing (in mM): 75 NaCl, 18 Na_3·citrate and 0.05% (v/v) Triton X-100. Cells were incubated with 100 μL of antibody buffer containing the appropriate secondary antibodies, rinsed 3 x 5 minutes in antibody wash solution and vacuum dried before mounting onto frosted glass slides (Surgiglass, 1.0 mm thick slide). Spherical aberration due to refractive index (η) mismatch was minimized by mounting cells with 8 μL of glycerol based mounting medium containing 90% (v/v)

glycerol, 10% (v/v) PBS and 2.5% (w/v) DABCO (1,4-Diazabicyclo-[2.2.2]octane, Sigma), an anti-fade reagent. Clear nail polish was used to seal the coverslip onto the slide. To determine non-specific binding, staining control experiments with secondary antibody without primary antibody were performed.

All antibody incubations were carried out at room temperature, unless indicated, and in a humidifier, to prevent dehydration. Primary antibodies were incubated for 4 hours, while secondary antibodies were incubated for 1.5 hours, unless indicated otherwise.

In this study, RyR and NCX were labelled sequentially because, as previously stated, both primary antibodies were mouse monoclonal. The first primary antibody (anti-RyR, 1:100) was masked by incubating with a large excess (200 μg/mL) of unlabeled goat anti-mouse Fab overnight at 4°C. After masking, the first secondary antibody donkey anti-goat IgG conjugated to Alexa 488 (1:100) was applied. Incubation with the first secondary was followed by incubations with the second primary antibody (anti-NCX, 1:300) and the second fluorescent secondary antibody, donkey anti-mouse conjugated to Alexa 555 (1:100). The control experiment skipped labelling with the second primary antibody and proceeded directly to the second secondary antibody. This allowed confirmation that all sites on the first primary antibody had been masked by the goat anti-mouse Fab. The optimal dilution factors for primary and secondary antibodies were determined by conducting dilution matrices.

2.4.3 Microscopy

Labelled cardiomyocytes were examined with a Zeiss LSM 5 Pascal Laser Scanning Confocal Microscope (LSCM) equipped with an Axiovert 200 M bp microscope (Carl Zeiss AG, Gottingen, Germany). Argon and Helium-Neon lasers provided the 488 nm and 543 nm excitation beams, respectively. The Argon beam was internally calibrated to emit 8 mW of laser light, while the Helium-Neon emitted 5 mW, neutral density filters were used to further attenuate the intensity of the laser light (to 1% and 50%, respectively). To minimize bleed through of signals, images were collected in multi-track mode, such that each fluorophore was excited, and its emission collected, sequentially. For each excitation beam, laser light was focused onto the sample through a highly corrected objective (Zeiss Plan-Apochromat 63X, numerical aperture (NA) of 1.4) in a diffraction-limited mode. Emitted light was directed via an XY scanner onto a dichroic beam splitter, which separated the emission from the excitation light (HFT 488, 543 for the respective light paths). The fluorescence from 543 nm excitation was sent directly to PMT 1(channel 1) after passing through a 560 nm long-pass filter, while the fluorescence emitted from the 488 nm excitation was directed to PMT 2 (channel 2) by a secondary dichroic beam splitter (NFT 545). Before reaching the PMT, the light signal was filtered with a 518 ± 13 nm band-pass filter. To optimize image acquisition, the pinhole was set to 1 Airy disk for each collection channel. The Z-interval (axial axis) was adjusted to 250 nm, the lateral axes (X and Y plane) were each set to 100 nm, in accordance with the Nyquist theorem, enabling optimal replication of the signal while reducing the possibility of sample photobleaching. A typical image stack consisted of 50-75 serial two-dimensional images acquired through the cell. The point spread function of the microscope was measured using Fluosphere, 220 nm diameter beads and

collected using a voxel size of 50nm X 50nm X 100nm (Molecular Probes, custom order). The three-dimensional data stacks were exported as 16-bit Tiff images for processing and analysis.

Exported TIFF images were deconvolved to reassign out-of-focus light by a maximum likelihood estimation (MLE) algorithm using Hugyens Pro 2.4.1 (Scientific Volume Imaging, Hilversum, Netherlands) software and subsequently imported into Imaris 4.0 (Bitplane Inc, Saint Paul, MN) for threshold setting and colocalization analysis. A threshold was set that removed ~98% of the signal found in control images from labelled images prior to analysis. 3-D images were then examined, voxel by voxel, to determine the degree of colocalization.

2.5 Data and Statistical Analysis

Statistical analysis was completed using SPSS 9.0 statistical software. Data were analyzed for outliers using boxplot analysis. Suspected outliers were examined prior to further analysis and were removed from the data set if values were considered questionable. Imaris 4.0 was used to independently analyze each voxel, from images within an age group, and to determine if it contained colocalized proteins or not. Two proteins were designated to be colocalized if the signals for both originated from within the same voxel.

Equality of the means of the degree of colocalization in the different age groups, for RyR or NCX were analyzed using a logistic regression in SPSS 9.0. Logistic regression is well suited for binary data as it contains non-normally distributed residuals.

Furthermore, logistic regression models the degree of colocalization as a function of age, enabling one to predict the degree of colocalization at any age.

CHAPTER 3: RESULTS

3.1 Immunoblots

Under reducing conditions, NCX1.1 usually appears on a Western Blot at apparent molecular masses of 160, 120 and 70 kDa, with the smaller fragment being considered a proteolytic fragment (Nicoll et al., 1990; Porzig et al., 1993). The R3F1 anti-NCX antibody detected polypeptides of 160 and 120 kDa in crude membrane extracts from ventricular tissue of neonate rabbits, indicating specific binding of the antibody to NCX1.1 (Figure 6).

The specificity of MA3-916 anti-RyR antibody has been previously characterized by Sedarat et al (Sedarat, 1999) in our laboratory. The antibody detects a single, high molecular mass band (565 kDa) in crude membrane extracts from ventricular tissue of neonatal rabbits. These data indicate that the selected antibodies bind specifically to the respective proteins and are suitable for use in this immunofluorescent study.

3.2 Immunocytochemistry

Alterations in NCX immunolocalization with development were examined using single stained ventricular myocytes. RyR immunolocalization and colocalization measurements were made on dual-labelled myocytes. As colocalization is a resolution-dependent descriptor, all images were deconvolved and binarized prior to analysis. The improvement in resolution realized with restoration, in both laser lines, is shown in Figures 7 and 8.

3.2.1 NCX Immunolocalization with Development

NCX immunolocalization pattern changed with development (Figures 9 and 10). At the earliest observed stage of development, 3-days, the NCX signal was highly concentrated along the cell periphery. The staining pattern was non-homogenous, suggesting that NCX may be clustered in distinct domains within the plasma membrane. In 3- and 6-day old myocytes, staining was clustered into areas of high and low concentration, with the strongest signal occurring toward the end of the cells. During development, NCX immunolocalization changed from being predominately peripheral, to occurring predominately intracellularly. The time course for internalization coincided with the advent of the T-tubular system (~10 days post-partum), suggesting that NCX was being internalized with the plasma membrane invagination. In fully developed myocytes (56-day old), the NCX staining pattern occurred along transverse bands and it appeared to be more spatially organized. NCX fluorescence was localized to the sarcolemma, intercalated discs, and T-tubule system. Intensity profiles from cell sections, created using custom software written in IDL by Eric Lin, highlight the changes seen in NCX immunolocalization with age (see Figure 9). In the profiles, peaks correspond to areas of high concentration. At 3-days post-partum, NCX fluorescence intensity was mainly peripheral with many peaks and valleys, corresponding to the clustering seen in the images. With development, the high intensity peaks were located in the intracellular region, additionally, the periodicity of the peaks increased in uniformity.

3.2.2 RyR Immunolocalization with Development

RyR immunolocalization was highly organized along the Z-lines of the contractile element even at the early stages of neonate development. At the earliest time point examined, 3-days post partum, the RyR signal was present in clear striations, which were regularly spaced at ~2 μm intervals, consistent with previous observations (Figure 10) (Sedarat et al., 2000). RyR staining was observed to occur at the cell periphery and intracellular regions. Although the strength of the RyR signal increased with age (consistent with increases in RyR concentrations expected with increased cell size), the immunolocalization pattern did not change. The well organized staining of RyR in the cytoplasm at 3-days and the lack of alteration in the staining pattern with development is supportive of the hypothesis that the SR is well developed shortly after birth.

3.2.3 Colocalization of NCX and RyR

The pattern of distribution of NCX and RyR colocalization was examined using merged images (Figure 10). In these images, voxels containing both RyR and NCX were pseudo-coloured yellow. Alterations in colocalization staining pattern with development mimicked changes seen in NCX immunolocalization. In 3-day old myocytes, before T-tubular development, colocalization appeared on the cell periphery, at the junction of RyR with the sarcolemma (Figure 11). With maturity, NCX immunolocalization began to appear in the cell interior; corresponding with the internalization of NCX was an increase in the number of colocalized voxels present in the intracellular regions. In 6- and 10-day old myocytes, colocalization was seen both along the cell periphery as well within the interior of the cell, suggesting that NCX coupled with RyR as its distribution altered with T-tubular development. In addition, as NCX staining became more evenly

distributed throughout the cell, the colocalization pattern did as well. Adult cardiomyocytes exhibited a pattern of colocalization that resembled striated transverse bands along the length of the entire cell. Within the cell, there are two populations of RyR, junctional and corbular, which are named according to the component of the SR on which they are situated. Junctional RyR is juxtaposed with the sarcolemma and is involved in E-C coupling, whereas corbular RyR contributes to SR Ca^{2+} release but is not in functional proximity with the DHPR (Carl et al., 1995). The parallel transverse banding of the colocalized voxels with the regular spacing of the RyR staining pattern suggests that NCX was colocalized with junctional or dyadic RyR. With age, there was a decrease in the signal-to-noise ratio of the NCX images and therefore these observed changes may be artifactual.

3.3 Data and Statistical Analysis

Imaris 4.13 was used to calculate the total number of RyR voxels, total number of NCX voxels and total number of colocalized voxels present in each cell. The percentage of NCX voxels colocalized with RyR and the percentage of RyR voxels colocalized with NCX was calculated using this software.

3.3.1 Percentage of Colocalization in the Different Age Groups

Channel statistics provided by Imaris were grouped according to cell age and the total number of voxels for each protein and the percentage of colocalization in the different age groups were calculated. The results are summarized in Table 2 and Figures 12 and 13.

Table 2: Number of NCX, RyR and colocalized voxels in the different age groups

Age	Number of Voxels*		
(Days)	NCX	RyR	Colocalized
3	17804	25562	4984
6	36250	29197	9404
10	33844	40713	14319
20	17906	39407	12540
56	28451	56273	18208

The percentage of RyR colocalized with NCX increased between 3- and 6-day old myocytes and then remained steady in older animals (Figure 12). In 3-day old myocytes, ~22 % of RyR was colocalized with NCX and colocalization was limited to the cell periphery. There was no significant difference in the RyR colocalization percentage between 6-, 10-, 20- and 56-day old myocytes. The pattern of colocalization did change in older animals, despite the fact that no changes in the colocalization percentage were apparent. In contrast to RyR colocalization, the percentage of NCX colocalized with RyR increased with developmental stage (Figure 13). Immature myocytes (3-, 6-, 10-days old) did not significantly differ from each other. In these myocytes, colocalization was restricted to the cell periphery, although internal couplings became evident as NCX immunolocalization in the cell interior increased, with the advent of the T-tubule system. At maturity, the NCX colocalization percentage increased significantly. Both 20- and 56-day old myocytes were significantly different from immature myocytes and from each other. Interestingly, the percentage of NCX colocalized was much larger than the percentage of RyR colocalized. This difference may be due to the disparities in the

number of voxels occupied by the respective proteins; RyR occupied a larger number of voxels than NCX. In addition, as previously mentioned, two populations of RyR exist in the cell, with only the junctional RyR being juxtaposed with the sarcolemma and capable of colocalizing with a membrane protein such as NCX.

3.3.2 Statistical Analysis

To examine the equality of means of the percentage of colocalization in the different age groups, a one-way analysis of variance (ANOVA) with an α-level of 0.05 was performed for both NCX and RyR. The F-statistic determined whether there was a difference between one or more means for both proteins. A significant difference in the percentage of NCX colocalized ($p<0.0001$) and in the percentage of RyR colocalized ($p<0.0001$) among the groups was identified.

Individual differences were examined using Gabriel post-hoc tests. The percentages of NCX colocalized in 20- and 56-day old myocytes were significantly different from all other age groups. RyR colocalization percentage differed significantly between the first age group (3-day old) and all other groups (Figures 12 and 13).

CHAPTER 4: DISCUSSION

4.1 Immunofluorescent Labelling

Immunofluorescence is a powerful tool for the identification of proteins in cells and tissues. The ability to discern the location of proteins within cells provides valuable insight into their function and interaction with other proteins. Immunofluorescence uses a fluorescent dye, such as fluorescein isothiocyanate (FITC), conjugated to an antibody to directly label a protein of interest, enabling it to be visualized with illumination under a microscope. Upon illumination with a either a mercury arc lamp or another type of light source of appropriate wavelength, the fluorescent dye will become excited and emit energy in the form of a specific wavelength of light which can be seen through the eyepiece of a microscope equipped with the appropriate filter cubes. There are many advantages to using fluorescent labels to detect antigens; mainly fluorescence provides an instantly visible label which, when viewed against a non-fluorescent background, may yield excellent contrast. The advent of numerous fluorescent dyes with a variety of excitation / emission spectra allows multiple antigens to be stained and viewed on a single specimen. However, as with any technique, a thorough understanding of potential sources of error and their effects on the validity of results is required.

4.1.1 Sources of Error in Indirect Immunofluorescent Labelling

Indirect immunofluorescence is a modification of the original directly labelled antibody method. It uses a combination of two or more different antibodies, an unlabelled primary antibody raised to the antigen of interest that is subsequently detected

by a second fluorescent-conjugated antibody directed toward immunoglobulin of the species in which the first antibody was raised. Indirect labelling has a higher sensitivity in comparison to directly labelling with a primary antibody that has been conjugated to a fluorescent molecule. The amplification in sensitivity occurs due to the availability of two antigen binding sites on the primary antibody, which can each bind labelled anti-immunoglobulin molecules. It is generally more economical to use indirect labelling because the second layer anti-immunoglobulin antibodies can be used to detect numerous primary antibodies generated from the same host species but directed towards different proteins. Furthermore, directly conjugating primary antibodies may negatively affect the antigen-antibody binding affinity, and can be an extremely expensive and time-consuming task (Allan, 2000; Burry, 2000; Larsson, 1988.; Polak, 2003.).

The many advantages of indirect immunofluorescent labelling have made it a valuable laboratory technique. However, this methodology is highly dependent on the specificity of antibodies, therefore it is important to run experimental controls, that ensure the detection system is correct and the primary antisera is responsible for the labelling pattern that is observed, especially when double immunostaining (Allan, 2000; Burry, 2000; Polak, 2003.). Additional problems arise when double immunostaining, leading to false positives, which are amplified when using primary antibodies from the same host species. The main concerns include cross-reactivity and non-specific binding of the primary and secondary antibodies as well as autofluorescence of the tissue / cells.

The most common reason for false positives would be cross-reactivity of the primary antisera with proteins intrinsic to the tissues being examined or recognition of the primary antibody by both secondary antibodies. A simplistic method for determining

specificity of an antibody includes the incubation of the antibody with its target protein or peptide, prior to application onto the tissue / cells. The elimination of a signal would indicate that the antibody is specific to its antigen. This control can demonstrate that the antibody binds to it target protein / peptide, but does not demonstrate that other intrinsic proteins are not bound, because the antibody is pre-absorbed only with its target antigen. A more rigorous control is the use of immunoblots. An immunoblot of a specific antibody would demonstrate that the antibody tested only recognizes protein of the appropriate molecular weight. If multiple proteins were detected, the antibody would be deemed to be cross-reactive (Burry, 2000). However, the possibility exists that an antibody may specifically detect the antigen of interest in an immunoblot but not in situ, for variety of reasons. Detection on an immunoblot requires denaturation of the protein, which increases the availability of antigenic sites. In situ these sites may be lost due to steric hindrance, tertiary structure of the protein, or its cellular location. Conversely, an antibody may cross-react with unknown protein on an immunoblot but not in situ (Allan, 2000).

A more valid control is the **E**nzyme-**L**inked **I**mmuno**S**orbent **A**ssay (ELISA), which is a method of testing antibody specificity using layers of antigens and antibodies, conditions that mimic those of immunocytochemisty. The first layer consists of coating the inner walls of micro-plate wells with known quantities of antigen; the second layer is the primary antibody to be tested, which is applied in a series of dilutions. Binding of the primary antibody to the antigen is detected with a third layer of antibody, that is directed against the species in which the primary antibody was raised, conjugated to alkaline phosphatase, which produces a coloured end product that can be detected upon

development with chromogen. The colour intensity indicates the amount of antigen-antibody complexes and can be quantified either by eye or with a spectrophotometer. Cross reactivity and contaminating antibodies are tested for by lining the wells with antigens that are structurally similar to the antigen of interest (Polak, 2003.).

Primary antisera may bind to tissue sites that do not contain the antigen of interest, this non-specific binding will be detected along with specific binding by the secondary antibody creating "background signal". Additionally, secondary antibodies may also bind non-specifically, and when double immunolabelling, the background signal from each individual staining is additive, increasing the noise in images and confounding results. Non-specific binding is usually significantly weaker than specific antigen-antibody binding, therefore prior knowledge of the conditions that contribute to its occurrence, enables the addition of steps into the experimental protocol to decrease its prevalence. To effectively minimize unwanted interactions, it is important to utilize techniques that prevent non-specific binding from both sources, the tissue and anti-sera (Allan, 2000; Larsson, 1988.; Polak, 2003.).

Non-specific binding may occur due heterogeneity of antisera. Antisera heterogeneity is more common in polyclonal antiserum, which usually contains a mixture of antibody subpopulations of different specificities and different avidities. The prevalence of the unwanted antibodies is easily minimized by affinity purification of the primary antisera in conjunction with the use of high dilutions. Dilution of the antisera with buffer reduces the concentration of the unwanted antibodies compared to the concentration of the specific antibody of interest (Larsson, 1988.; Noorden, 1983.; Polak, 2003.).

The major tissue-specific factors that lead to non-specific binding are (1) charged amino acid residues that attract antibodies with opposing charges, (2) hydrophobic attractions between immunoglobulins and tissue, and (3) receptors, within the tissue, for the Fc portion of antibodies. The simplest remedy is to block potential binding sites by incubating the tissue or cells with normal (non-immune) serum before applying the primary antibody. Normal serum contains natural antibodies and other proteins that can occupy the binding sites. When using indirect labelling, it is critical to use normal serum from the species that provides the secondary antibody. If serum from the same species as the first antibody is used, it can effectively block non-specific binding of the first antibody but will result in extra deposits of immmunoglobulin antigen for the second, anti-species immunoglobulin, creating background staining. Serum from the host of the secondary antibody will block non-specific binding of the primary antiserum equally well and cannot be immunoreactive to the immunoglobulin of its own species. Alternatively blocking can be accomplished by adding an "inert" protein such as bovine serum albumin (BSA) or casein, milk protein, in a 1% or 2% solution in buffer; however, these proteins will not occupy Fc receptors sites. The addition of detergent in the washing solution can also prevent non-specific binding, because the bonds are much weaker. A combination of the these methods is commonly used to ensure that charged amino acids as well as Fc receptors sites are often bound by the addition of non-immune proteins (i.e. normal serum, BSA or casein) in the buffer (Allan, 2000; Larsson, 1988.; Polak, 2003.).

Many cells and tissues exhibit autofluorescence when viewed under different excitation wavelengths. This cellular autofluorescence is due not only to the presence of endogenous biomolecules, but is also produced by fixation; aldehyde fixatives react with

amine groups and proteins to create fluorescent products. The spectral range of autofluorescence created by biomolecules is typically quite broad compared to the spectra of the dyes, probes and proteins that most researchers are interested in, therefore it is difficult to eliminate by switching probes or by using traditional filtering methods. Some researchers have found success counterstaining with reagents such as sudan black, propidium iodide, or pontamine sky blue to significantly reduce autofluorescence. Fixation-induced autofluorescence can be decreased by limiting the length of fixation time, and by providing bland amine groups to quench the fixation, i.e. glycine (Allan, 2000; Polak, 2003.).

4.2 Immunofluorescence of RyR and NCX

4.2.1 RyR Staining Pattern

The adult phenotype of RyR immunolocationization has been well characterized in cardiac and skeletal tissue of many animal types. Carl et al (Carl et al., 1995), used confocal microscopy and electron microscopy to examine the distribution of RyR in cryosections of adult rabbit ventricular tissue (Carl et al., 1995). The predominant RyR immunofluorescence staining pattern was transversely oriented punctate bands, evenly spaced at ~2 μm intervals, which were present along the whole length of the cell. This spacing is consistent with the distribution of the T-tubules, which are located along the Z-lines of ventricular myocardium (Carl et al., 1995). To support the location of RyR at the Z-lines, the investigators co-stained sections for RyR and myosin, which is the predominant protein of the A band, and found no overlap of signal between the proteins. A similar immunostaining pattern of RyR was detected by Scriven et al, in their study examining the localization of contractile proteins in adult rat ventricular tissue (Scriven et

al., 2000; Scriven et al., 2002). We observed a staining pattern of RyR that is consistent with the established RyR immunostaining pattern in adult cardiac cells.

Few studies have been published examining the developmental status of the SR via immunostaining of SR membrane proteins (Haddock et al., 1999; Perez et al., 2005; Sedarat et al., 2000). In the current study, no difference was observed in the distribution of RyR during post-natal development of rabbit ventricular myocytes, in comparison to adult ventricular cells, consistent with previously published findings from our lab (Sedarat et al., 2004; Sedarat et al., 2000). The strong and well-defined fluorescence signal arising from RyR in ventricular myocytes from 3-day old rabbits is indicative of a SR that, shortly after birth, is at a stage of development more advanced then previously thought. A recent study by Perez et al, examined the structural organization and maturity of the SR by evaluating the cellular distribution of SERCA2a in newborn rat heart (Perez et al., 2005). The immunostaining pattern of SERCA2a in ventricular myocytes from 2-day old rats was well-organized, exhibiting a distribution that was oriented transverse to the longitudinal axis of the cell with a regular 2 μm spacing (Perez et al., 2005). The finding that two different SR membrane proteins are spatially organized in the very early post-natal stages provides significant evidence supporting the hypothesis that at birth, the SR is structurally well developed in mammalian ventricular myocytes.

4.2.2 NCX Staining Pattern

In rabbit adult myocytes, NCX immunostaining was observed in the sarcolemmal membrane, intercalated discs, and T-tubule membrane. The fluorescent signal was strong and appeared in a regular striated pattern, which was transversely oriented to the long axis of the cell, similar to the pattern displayed by RyR and DHPR suggesting that NCX

is localized to the Z-lines of the sarcomeres (Scriven et al., 2000; Sedarat et al., 2000). The observed staining pattern is in agreement with previous studies on adult rat and guinea pig myocytes (Frank et al., 1992; Kieval et al., 1992). Kieval et al (Kieval et al., 1992) found that NCX labelling appeared as a regular array of fluorescent foci, in both guinea pigs and rats, which overlapped with vinculin, a cytoskeletal protein that interacts with actin, supporting the localization of NCX along the Z-line of the sarcomeres. In adult myocytes, and throughout development, we observed that the intercalated discs exhibited intense fluorescent signal. Kieval et al (Kieval et al., 1992) also found that both guinea pig and rat adult myocytes displayed a high signal intensity in these areas. They postulated that the high-intensity signal was due to the increased surface area created by infolding of the sarcolemma, which is characteristic of the intercalated discs. An earlier study by Frank et al (Frank et al., 1992) a found strong immunofluorescent labelling in the T-tubule, although they observed patchy labelling of the peripheral sarcolemma, and only 50% of the observed cells showed intense labelling of the intercalated discs. These differences are most likely due to the use of different antibodies towards NCX, by all three groups, which were used in different concentrations (Frank et al., 1992). We used a monoclonal IgG, Frank et al (Frank et al., 1992) used a monoclonal IgM, while Kieval et al (Kieval et al., 1992) used a polyclonal IgG. Previous studies have found the nuclei to be void of NCX labelling, which is consistent with our observations (Frank et al., 1992; Kieval et al., 1992).

The developmental expression of NCX has been previously examined by two different laboratory groups (Chen et al., 1995; Haddock et al., 1999). Both groups of researchers observed homogeneous staining of NCX on the peripheral sarcolemma of

neonate myocytes and found the spatial organization of NCX changed during ontogeny. We observed a similar alteration in the spatial organization of NCX immunostaining with development. Additionally, the fluorescent signal of NCX had a stronger intensity in neonate myocytes than in adult myocytes, which is in agreement with the decreased expression level of NCX that occurs with development (Artman, 1992). To compensate for the known decrease in NCX expression, the previous studies increased the concentration of the anti-NCX antibodies used to stain myocytes from older animals (Chen et al., 1995; Haddock et al., 1999). Contrary to previous findings, we observed NCX immunostaining pattern in neonates that was non-homogeneously distributed along the sarcolemma.

The staining pattern observed by Haddock et al, is questionable due to possible experimental error, as will be discussed in further detail in the next section (Haddock et al., 1999). Discrepancies between our findings and that of Chen et al, may be due to differences in antibody concentrations used for labelling, different sampling frequencies during image acquisition, and differences in cell health (Chen et al., 1995). Both studies used the R3F1 NCX antibody, however, we used a higher dilution (1:300) in comparison to the other study (1:200). The optimal working dilution is important to determine, as the dilution providing the brightest fluorescence often does not provide the best resolution of detail. Higher dilutions may result in better definition of staining and decrease the background noise (Larsson, 1988.; Petrusz, 1982). We found that at a dilution of 1:300, we were able to reduce the degree of background and non-specific staining.

More importantly, poor cell health will adversely affect the labelling pattern. Both our study and that of Chen et al, examined ventricular myocytes of rabbits but at

slightly different developmental stages; 3-, 6-, 10-, 20- and 56-days old and 5-, 11-, 17-, 30 and 90-days old, respectively (Chen et al., 1995). The isolation of healthy myocytes from rabbits under 10-days of age is extremely difficult due to the small size and developmental immaturity of the hearts. Immature cells are more sensitive to the digestive enzymes and less resistant to the stress induced by the isolation and fixation procedures, requiring solutions and digestion times to be adapted accordingly. Healthy and structurally intact neonatal cells should appear as narrow rod-like cylinders with tapered ends. The images of 5-day old myocytes published in the study of Chen et al, displayed cells with blunt ends, which may indicate that the cells were ruptured or torn, in addition to cells that displayed significant curvature of the peripheral sarcolemma. Cell curvature is indicative of a myocyte that is in a state of permanent contraction, known as a contracture. If NCX is indeed located at the Z-lines, as it has been suggested, contracture of the cell may result in the appearance of a homogenous immunostaining pattern of NCX. The agreement of our results in myocytes from juvenile and adult rabbits, which are more resistant to processing, is supportive of this theory. The NCX immunostaining pattern in myocytes from 10-day old rabbits is similar to the pattern reported in 11-day myocytes by Chen et al. The alterations in the organization of the sarcolemma labelling started to occur with the emergence of short transversely oriented fluorescent bands, which most likely concurred with the advent of the T-tubule system. Myocytes from 20-, 30- and 56-day myocytes had NCX immunofluorescence that was distributed over the peripheral sarcolemma and the T-tubules as punctate bands (Chen et al., 1995).

4.2.2.1 Implication for E-C Coupling

The function of NCX in maintaining calcium homeostasis of the adult ventricular myocytes on a beat-to-beat basis has been well established (McDonough et al., 2002; Philipson and Nicoll, 2000). The strong immunofluorescent signal of NCX throughout the T-tubular system and the peripheral sarcolemma underscores its importance in this function. The juxtaposition of the exchanger with the Z-lines of the sarcomere will enable it to quickly respond to changes in $[Ca^{2+}]_i$ that occur with CICR. The higher concentration of NCX protein during fetal and neonatal periods, as well during senescence, suggest that it may play an increased role in relaxation and perhaps cell contraction during these periods (Artman, 1992; Koban et al., 1998; Qu et al., 2000). The non-homogenous distribution of NCX in neonate myocytes may facilitate Ca^{2+} homeostasis in the developing myocardium if it is localized within sarcolemmal microdomains, along with other ion-transporters and calcium handling proteins. Sarcolemmal caveolar microdomains may provide this requisite domain.

Caveolae are small cave-like invaginations of the plasma membrane and are characterized by the presence of caveolin, a scaffolding protein integral to the formation of caveolae (Figure 14). The cardiac-specific isoform, caveolin 3 (Cav3), has been shown to be associated with both the plasma membrane and the T-tubules of cardiac myocytes (Parton et al., 1997; Song et al., 1996; Tang et al., 1996). In addition to Cav3, caveolae often contain glycosylphosphadidylinositol (GPI)-anchored proteins, transmembrane proteins, enzyme kinases, α-adrenergic signalling molecules and G-proteins (Drevot et al., 2002; Fujita et al., 2001; Hoessli et al., 2000; Ilangumaran et al., 1999; Kovarova et al., 2001; Simons and Ikonen, 1997). This composition is conserved

between species and cell lines, supporting the idea that caveolae have an essential role in cellular processes (Okamoto et al., 1998; Xu et al., 2001).

There are several lines of evidence suggesting that in neonate myocytes caveolae may be functioning as a microdomain that serves to promote the interaction of proteins involved in E-C coupling. It has recently been demonstrated by Yarborough et al (Yarbrough et al., 2002) that cardiac voltage-gated sodium channels are associated with caveolin-rich membranes obtained by detergent-free buoyant density separation and Cav3 antibodies were able to immunoprecipitate the channel proteins. In the same study, indirect immunofluorescence and immunogold transmission electron microscopy suggested that the two proteins colocalized with each other, although sophisticated image analysis was not done. Additionally, the interaction of NCX and Cav3 has been shown to occur in bovine sarcolemmal vesicles using sucrose density gradients and co-immunoprecitipation (Bossuyt et al., 2002).

4.2.3 RyR and NCX Colocalization

The principal aim of this study was to determine if NCX and RyR are positioned in neonatal ventricle myocytes such that functional communication can occur and if their localization respective to one another were altered with development. Colocalization analysis revealed that the percentage of NCX colocalized with RyR increased significantly with development, while the percentage of RyR colocalized with NCX significantly increased between 3- and 6-day old myocytes and then remained constant. The structural relationship of NCX and RyR has been previously been studied in adult rat ventricular myocytes, where they were shown to occupy separate domains, and during development in rabbit ventricular myocytes, where it has been suggested that the co-

incidence of NCX and RyR increased with development (Haddock et al., 1999; Scriven et al., 2000). Our results indicate that NCX and RyR colocalization may increase with development, mostly between developmental day 10 and 20. In fact, the percentage of NCX colocalized with RyR increased from ~20% in 10-day old myocytes up to 52% in adult myocytes which, as demonstrated so elegantly by Scriven et al (Scriven et al., 2000), nears the maximum degree of colocalization (~68%) that can be measured using immunofluorescence techniques (Scriven et al., 2000). This would suggest that the both our results and those of Haddock et al (Haddock et al., 1999) are spurious or that the results of Scriven et al (Scriven et al., 2000) are erroneous. There are several lines of evidence, which would suggest the former is true.

Images published by Haddock et al (Haddock et al., 1999) showing labelling of both NCX and RyR during development are inconsistent with previously published images of either protein. Three published studies, including our laboratory's previous findings, have used the mouse anti-RyR antibody from Affinity BioReagents (MA3-916) to examine RyR distribution in ventricular myocytes. All three investigative groups looked at adult ventricular myocytes and reported RyR to be located in regular arrays with rows of fluorescent foci distributed along the Z-line. The fluorescent signal was observed to be very strong at the foci, and little label was detected elsewhere in the cell (Scriven et al., 2000; Scriven et al., 2002; Sedarat et al., 2000). We have previously reported that during development the pattern of RyR immunolocalization does not change, which was corroborated by the present findings. Furthermore, RyR distribution in chick embryos and rabbit atrial myocytes, which lack T-tubules, also exhibit an immunostaining pattern that is well organized into regularly spaced foci. In comparison,

the RyR staining pattern published by Haddock et al (Haddock et al., 1999) was very diffuse, highly unorganized, and had a very low signal-to-noise ratio, as evidenced by the large amount of background noise present in the images. Additionally, their observed staining pattern did not correlate with their own finding of a highly developed and functional SR in neonatal myocytes, which was capable of Ca^{2+} release upon the application of caffeine (Protasi et al., 1996).

We have reported an immunofluorescent labelling pattern of NCX that is in partial disagreement with previous publications, including that of Haddock et al (Haddock et al., 1999). The observed staining patterns are dissimilar in only one age group, that of the early neonate (3- and 6-day old rabbits). The immunolocalization of NCX in juvenile and adult rabbit (10- through 56-day old) ventricular myocytes are comparable with others. In contrast, the pattern observed by Haddock et al (Haddock et al., 1999), once again, had a low signal-to-noise ratio, exhibited diffuse staining, and contained smears of fluorescence. Furthermore, the representative neonate cell images that were published exhibited cells that have curled or rounded ends, signifying disrupted cell structure (Chen et al., 1995; Frank et al., 1992; Haddock et al., 1999).

The staining pattern observed by Haddock et al (Haddock et al., 1999), is most likely the result of an erroneous experimental protocol. The choice of antibodies that are (1) specific to the proteins of interest (NCX and RyR), (2) are suitable for the intended application (immunocytochemistry) and (3) will not react with the species being studied (rabbits) limits the selection to two well characterized monoclonal antibodies. This required the investigators to use select a method with which to distinguish between two primary monoclonal antibodies raised in the same host species. They chose to take

advantage of the availability of an anti-NCX antibody, raised in a C2C12 cell line, which differed from the anti-RyR antibody in its class of immunoglobulin, IgM. This difference in isotype enabled the researchers to differentiate between the anti-NCX and anti-RyR primary antibodies by labelling them with isotype specific secondary antibodies. However, some problems may arise when using this methodology. Isotype specific antibodies may not be truly specific; therefore, it is important to run parallel single stained cells, as well as a number of controls to ensure cross-reactivity does not occur. Additionally, cross-reactivity could have been prevented by adapting the method of cell labelling. When dual-labelling the primary antibodies are commonly co-incubated, however a better approach would be to label cells sequentially with the application of a block (i.e. excess normal serum) between the incubation of the first secondary and the second primary antibodies, to ensure that all antigen binding sites are saturated. In this study, myocytes were co-incubated with both primary antibodies, while secondary antibodies were applied sequentially, hindering the ability to ascertain if the secondary antibodies were able to discriminate between isotypes (Allan, 2000; Haddock et al., 1999; Polak, 2003.).

The apparent low signal-to-noise ratio of the published images may also be a consequence of the choice of immunocytochemical protocol. The number of isotype specific antigenic sites on a primary antibody may be few, resulting in a weak signal. Additionally, the molecular weight of an IgM antibody is around 600 kDa larger than an IgG, thereby inhibiting its ability to bind due to steric hindrance, as well as possibly preventing the binding of the IgG antibody, especially if they are within the same domain (Larsson, 1988.; Noorden, 1983.). These last two obstacles can be overcome by ensuring

the complete permeabilization of cell membranes, sequentially labelling, with the IgG antibody being applied first, and using incubation times ranging from 4-24 hours to ensure full accessibility of the antibodies to the antigens. In the paper by Haddock et al (Haddock et al., 1999), the co-incubation of primary antibodies combined with a short incubation time, the primary antibodies were only incubated for 60 minutes at room temperature, created conditions, which would likely be insufficient to ensure adequate accessibility (Haddock et al., 1999). A 4-hour or overnight incubation at 4°C would have more likely enabled the primary antibodies to have sufficient accessibility to the antigens. Efficient binding of the antibodies would have a significant effect, in the positive direction, on the signal-to-noise ratio of the images.

Both our study and that published by Haddock et al performed double immunostaining with primary antibodies from identical host species (two monoclonal antibodies). Numerous problems arise when attempting to perform double immunostaining with antisera from the same host. Haddock et al (Haddock et al., 1999), used primary antibodies of different immunoglobulin classes, IgG and IgM, which requires highly specific secondary detection systems, whereas we attempted to change the species on the first primary antibody via the application of non-conjugated goat anti-mouse Fab fragments, which are monovalent. Although numerous controls were conducted to ensure complete blockage, the possibility of cross-reactivity of the secondary detection system between the two primary antibodies, due to insufficient block, exists. A confounding factor was the decrease in NCX protein expressed with age. Previous studies examining the distribution of NCX were primarily interested in a qualitative assessment of the localization of NCX in the cell and compensated for its

decrease in expression levels by increasing the amount of antibody used (up to 100-fold more). As we were primarily interested in quantifying the immunolocalization changes that may occur with development, all conditions were kept constant between age groups, from the concentration of antibody used to the imaging parameters (including the dynamic range of the images) with which the images were collected. This posed significant problems as the signal-to-noise ratio in images depicting NCX immunolocalization decreased with age, most likely a consequence of the decrease in protein expression levels (Artman, 1992). Therefore, it may be that there is no change in percentage of NCX colocalized with RyR, and that the increases seen are due to either cross-reactivity, increased noise, or a combination of both.

While understanding that contamination of the signal may have occurred, and that the presented results are inconclusive, the possibility exists that further studies may demonstrate that, in rabbits, the percentage of NCX colocalized with RyR does increase during development and the discrepancy between this finding and that of Scriven et al, must be examined (Scriven et al., 2000). NCX and RyR immunofluorescence was determined to be colocalized if both signals originated from the same voxel space of 100nm X 100nm X 250 nm. This voxel size would place the two proteins into the same microdomain, but localization within the same voxel does not necessarily equate to functional proximity. The efficacy of interactions between DHPR and RyR were demonstrated using functional experiments, which were supported with evidence from structural / imaging studies that placed the proteins within the same domain (Huang et al., 2004). During E-C coupling in the adult myocyte, NCX is primarily responsible for the removal of an amount of Ca^{2+}, which is approximately equal to that which enters via

DHPR during CICR. The contribution of transsarcolemmal Ca^{2+} to the total Ca^{2+} responsible for contraction in adult mammalian species ranges from 8% in murine cardiomyocytes to 30% in cardiomyocytes from most other adult mammals species, including humans. Thus, it is quite possible that NCX and RyR do not colocalize in the adult rat heart, where a relatively small amount of Ca^{2+} must be efficiently removed from the fuzzy space, but do colocalize in adult ventricular myocytes of rabbits, in which the contribution of transsarcolemmal Ca^{2+} is notably greater.

The dramatic increase in the degree of colocalization that occurs at 20-days post-partum nears the maximum percentage of colocalization that is detectable, suggesting that in the older age groups, the mouse anti-RyR antibody was not fully converted to a goat IgG and that quite likely, the degree of NCX colocalization with RyR did not appreciably change with development. However, there can be substantial changes in the relationship between NCX and RyR without any changes in the degree of colocalization due to alterations in the localization and expression levels of NCX with development. At birth, NCX is primarily located along the peripheral sarcolemma, whereas in adulthood, it is present throughout the peripheral sarcolemma and the T-tubule system. The density of NCX on the sarcolemma of neonatal myocytes will be higher than the density in the T-tubules of adult myocytes resulting from the combined effects of increased cell size and decreased expression. Therefore, it follows that in the neonate, at the points of NCX and RyR coupling, the density of NCX may be significantly greater, increasing the amount of Ca^{2+} influx with reverse mode operation that is available to activate RyR. In the adult, the decreased density of NCX at the site of coupling would diminish its role in activation. If the primary role for NCX in the adult is Ca^{2+} removal, it may not be necessary for it to

be localized within the fuzzy space, but simply being adjacent to it may suffice. A further note in support of NCX colocalization with RyR and possibly DHPR, is its ability to work synergistically with DHPR to increase Ca^{2+} influx in response to PKA simulation and its apparent role in Ca^{2+} influx during E-C coupling of failing human heart (Dipla et al., 1999; Viatchenko-Karpinski et al., 2005).

4.2.3.1 Implications for E-C Coupling during Development

Several recent studies have demonstrated that the SR is highly developed at birth and is capable of Ca^{2+} release, although its contribution to excitation contraction in the neonate is unclear. The greater cardiomyocyte surface-to-volume ratio, the extended plateau of the action potential and the decreased concentration of the DHPR, has led to the belief that the neonatal ventricular myocyte is much more dependent on extracellular calcium for contraction than the adult heart. This hypothesis has been supported by functional data, which has suggested that NCX may play an increased role in calcium homeostasis during early morphogenesis (Artman, 1992; Artman et al., 2000; Huang et al., 2004; Huynh et al., 1992; Wetzel et al., 1993; Wetzel et al., 1995). Unexpectedly, we found an increase in the percentage of NCX colocalized with RyR during ontogeny and although there is some uncertainty in the validity of the current findings, they may be correct and their implication needs to be examined.

If the percentage of NCX colocalized with RyR increases with age, this may suggest that its plays a greater role in the cessation of CICR than previously thought or that its role in the initiation of contraction is not decreasing. The simplest explanation for the increase in the percentage of NCX colocalized, is that there is a lower concentration of NCX in older animals, and that its predominate role in relaxation requires it to be

colocalized with RyR. Alternatively, the increase in colocalization does not dismiss the contribution of NCX to contraction during the neonatal periods but instead highlights it possible participation in halting SR Ca^{2+} release.

The mechanism that terminates CICR still eludes researchers. The current hypotheses focus on RyR inactivation mechanisms or SR Ca^{2+}depletion, which occur *after* contraction. DHPR and RyR have a well-established functional proximity that is much closer than the 100nm X 100nm X 250 nm voxel space in which they have been colocalized. This extreme closeness enables the fast and efficient communication that underscores CICR. NCX, which has been credited with primarily removing an amount of Ca^{2+} that is equivalent to the amount of Ca^{2+} that enters via DHPR during E-C coupling, may be present in the same microdomain, albeit outside the partnership of DHPR and RyR. The presence of NCX in this microdomain may allow the removal of Ca^{2+} creating a local depletion, similar to the local rise, such that the RyR cluster deactivates, leading to a wave of deactivation that follows the Ca^{2+} wave. It would be intriguing to examine how the presence of calcium-handling proteins within the same microdomain affects the mechanism of CICR termination.

The emergence of the adult phenotype of E-C coupling corresponds with the maturation of the cell architecture and does not "switch" phenotypes at a given juncture but instead evolves through a convergence of the phenotypes. During the fetal periods, NCX operating in reverse-mode may be able to bring in sufficient Ca^{2+} to induce contraction, however as the cell structure develops in size and complexity, SR Ca^{2+} release via RyR is recruited to facilitate contraction. At some stage of development, DHPR and NCX may act simultaneously to bring in transsarcolemmal Ca^{2+} that triggers

SR Ca^{2+}. At maturation, DHPR and RyR function to initiate contraction, and NCX contributes to relaxation and possibly to cessation of CICR.

CHAPTER 5: CONCLUSIONS

Adult myocardial function depends on systems which tightly regulate cytosolic Ca^{2+} ($[Ca^{2+}]_i$) on a beat-to-beat basis. However, these systems are underdeveloped in mammalian neonate cardiomyocytes, suggesting an altered E-C coupling mechanism is present at birth, which adapts with age, to the adult phenotype. It has been suggested that NCX may play a prominent role in E-C coupling of the neonatal heart by regulating Ca^{2+} influx via reverse mode activation to either (1) initiate contraction directly or (2) to initiate CICR via activation of SR Ca^{2+}release. Functional studies examining NCX exchange activity in neonatal rabbit ventricular myocytes found the peak velocity of Ca^{2+} extrusion by NCX (V_{NCX}) in response to caffeine-induced SR Ca^{2+} release was reached before the peak of the Ca^{2+} transient, as sensed by Fluo-3. This time delay was significantly greater in younger myocytes, suggesting that NCX is localized in the same microdomain as RyR (Huang et al., 2004). Therefore, the overall purpose of the current project was to examine if a structural relationship existed between NCX and RyR in the neonate, such that Ca^{2+} influx via reverse mode activation could initiate SR Ca^{2+} release and to examine if this relationship changes with development. The major findings of this study were:

1. NCX localization is clustered along the plasma membrane of neonate ventricular myocytes prior to T-tubule development. With development, NCX intracellular localization increases.

2. RyR localization appears to be highly organized throughout the cell, as early as 3-days post-partum birth and during development, suggestive of a fully developed SR system.

3. During postnatal development, the degree of NCX colocalization with RyR increases and during this period the pattern of colocalization staining between NCX and RyR changes from primarily peripheral to internal couplings. The increase in the percentage of NCX colocalized may be a result of incomplete blocking and / or a decreased signal to noise ratio.

The current analysis of colocalization is reflective of whole cell changes occurring with ontogeny. Whole cell analysis may not accurately reflect changes occurring along the periphery or within microdomains where CICR is believe to occur. Further analysis of colocalization in discreet domains may better illustrate the structural changes occurring during ontogeny.

APPENDIX: FIGURES

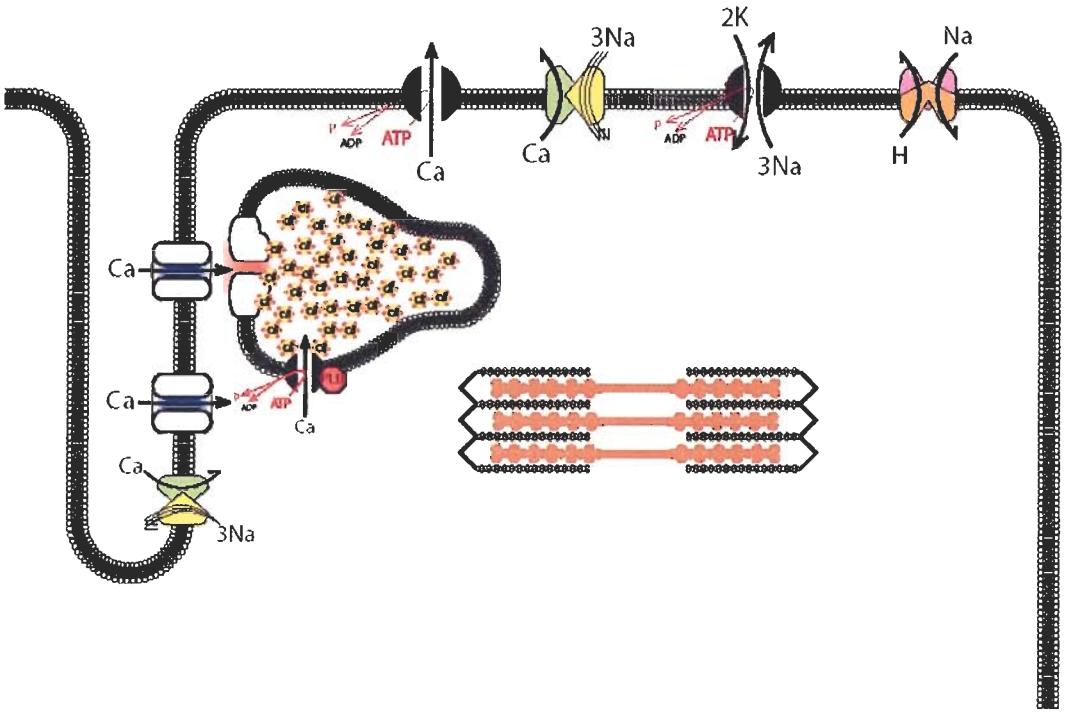

Figure 1. Excitation Contraction Coupling in the Adult Mammalian Heart.

Schematic Representation of E-C coupling in the adult myocardium. After from Bers (Bers, 2002) by Eric Lin.

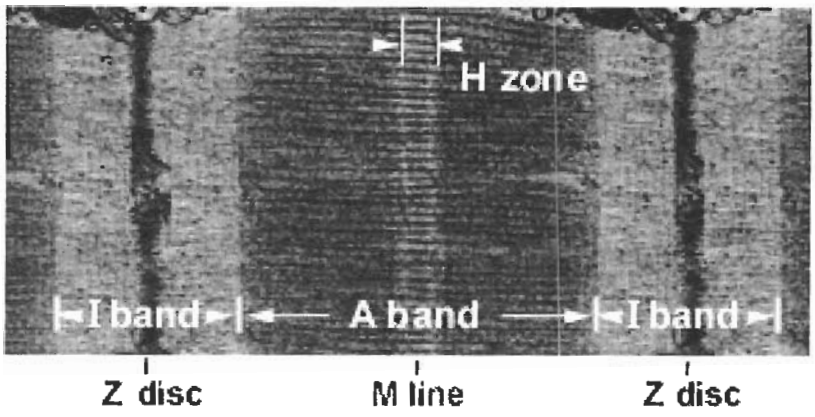

Figure 2. Ultrastructure of the Sarcomere.

This high magnification micrograph shows a single sarcomere. A sarcomere is the contractile unit of a myofibril and is bound on either side by the Z-disc. The I-band extends out from the Z-disc and is formed by the thin filament, which contains primarily the protein actin, but also troponin and tropomyosin. The I-band has a lighter appearance due to the lack of overlap with the thick filaments. The thick filaments compose the A-band and contain the protein myosin. The A-band is intersected by the H-zone, where there is no overlap of the thick and thin filaments. The dark-staining proteins making up the M-line are important in stabilizing the positions of the thick filaments.

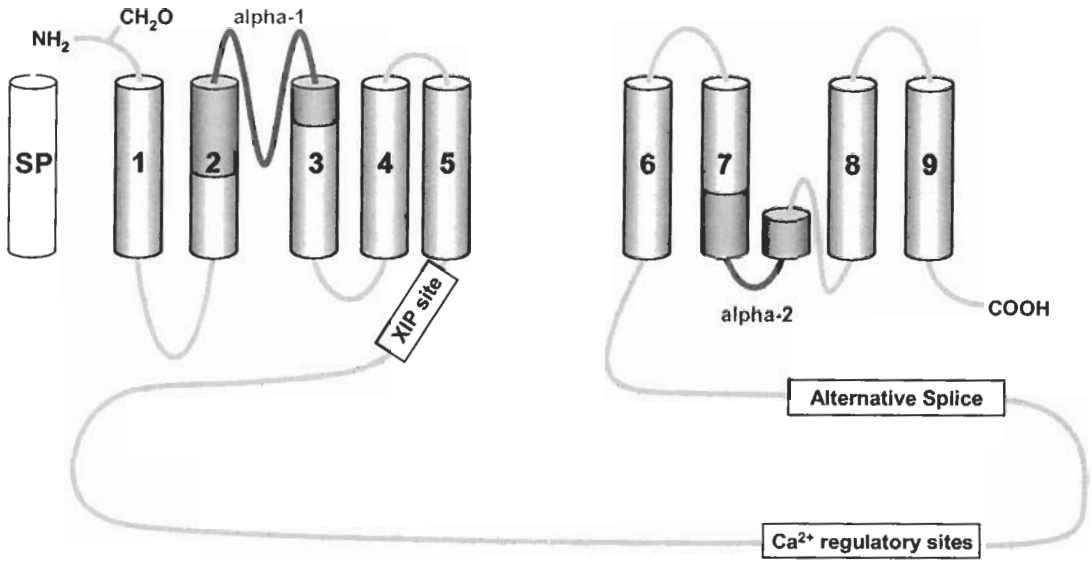

Figure 3. Putative Topological Model of the Na^+/Ca^{2+} Exchanger (NCX).

A putative model of the structure of NCX based on experimental evidence by Nicoll et al (Nicoll et al., 1999), and Iwamoto et al (Iwamoto et al., 1999)

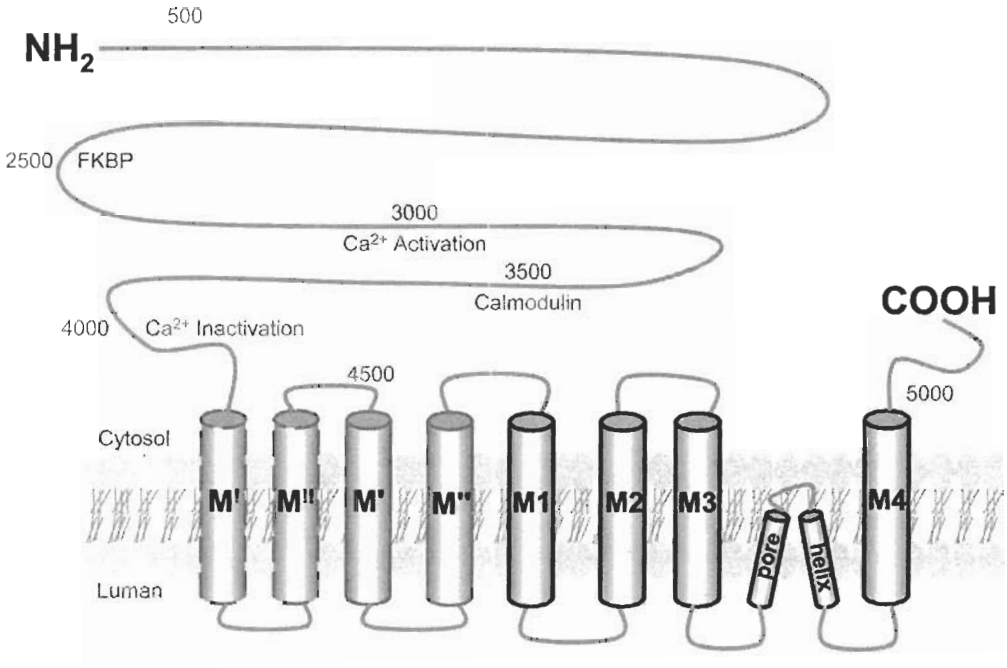

Figure 4. Schematic of the Putative Topological Models of the Ryanodine Receptor (RyR) in the SR membrane.

RyR was originally modelled to have four transmembrane domains, M1-M4. Subsequent studies using deletion mutants and epitope availability have suggested the presence of at least two additional domains, M′, M″, with the possibility of four, M^{I} M^{II} (Du et al., 2002; Takeshima et al., 1989; Tunwell et al., 1996; Zorzato et al., 1990).

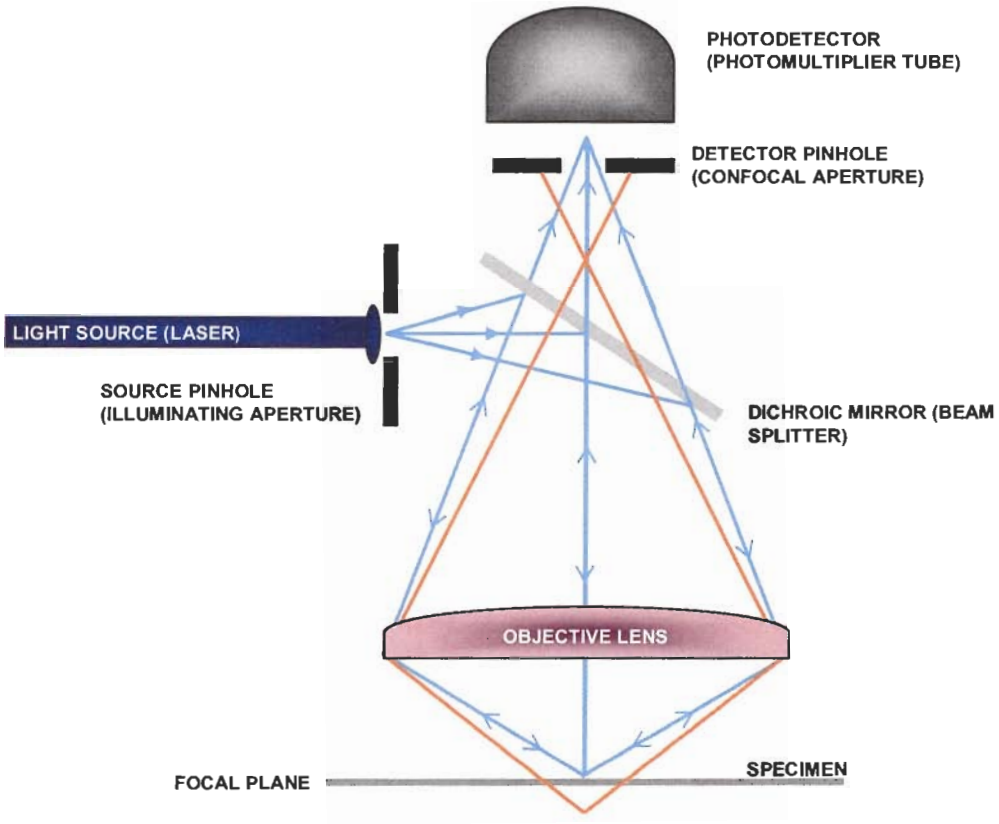

Figure 5. Simplified Optics of a Laser Scanning Confocal Microscope (LCSM).

The ray diagram of a simplified LSCM arrangement illustrates how a pinhole is used to focus light (blue lines) onto a focal plane of the specimen and converge onto the photodetector. Out-of-focus rays (orange lines) from planes above and below the central plane of focus are prevented from reaching the detector by the confocal aperture.

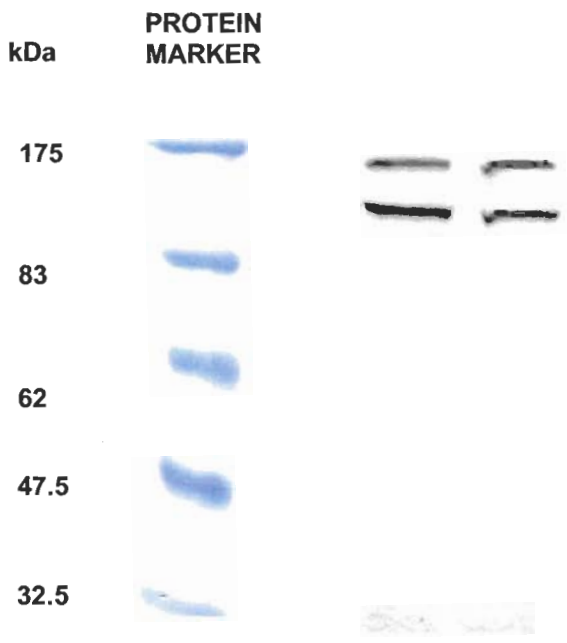

Figure 6. NCX Immunoblot

Western blot of neonatal rabbit ventricular muscle probed with R3FI anti-NCX antibody detected two bands at apparent molecular weights of 160 and 120 kDa consistent with the expected molecular weight for NCX.

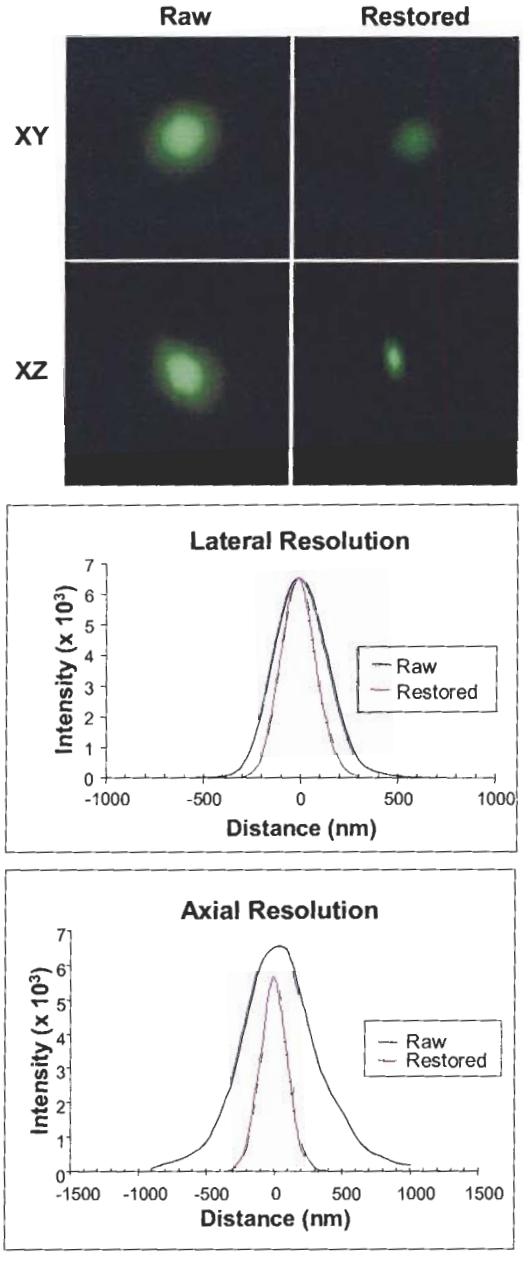

Figure 7. Affect of Deconvolution on a Bead Image (PSF)

The top panel shows the XY and XZ profile of a 220 nm fluorescent bead imaged with the 488 nm laser line before and after restoration with a MLE algorithm using Hugyens Pro 2.4.1 (Scientific Volume Imaging, Hilversum, NL). Below are graphs of the Airy disk intensity profiles. Resolution in both the lateral and axial planes were improved as seen by the full width half maximum (FWHM).

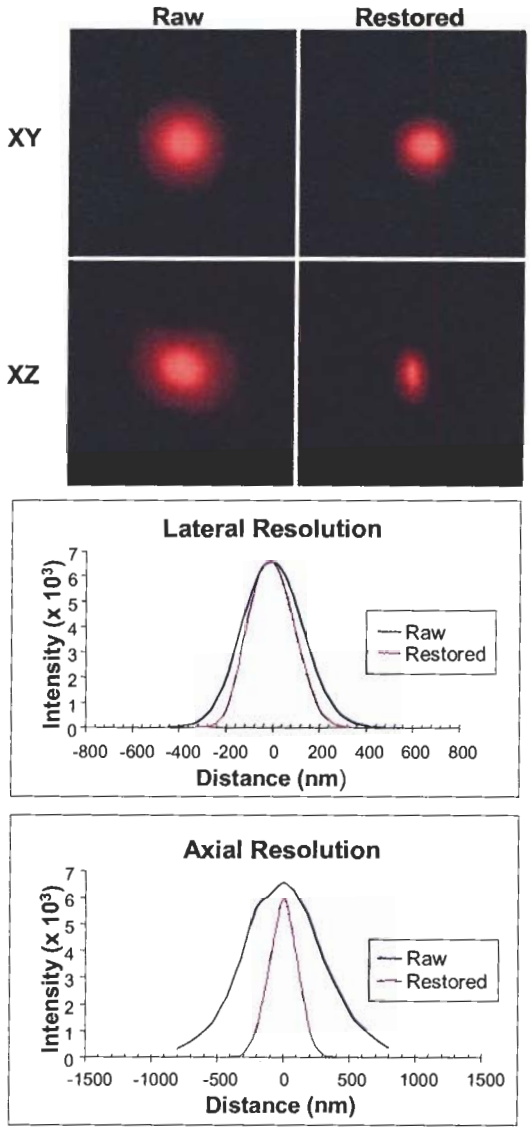

Figure 8. Affect of Deconvolution on a Bead Image

The top panel shows the XY and XZ profile of a 220 nm fluorescent bead imaged with the 543 nm laser line before and after restoration with a MLE algorithm using Hugyens Pro 2.4.1 (Scientific Volume Imaging, Hilversum, NL). Below are graphs of the Airy disk intensity profiles. Resolution in both the lateral and axial planes were improved as seen by the full width half maximum (FWHM).

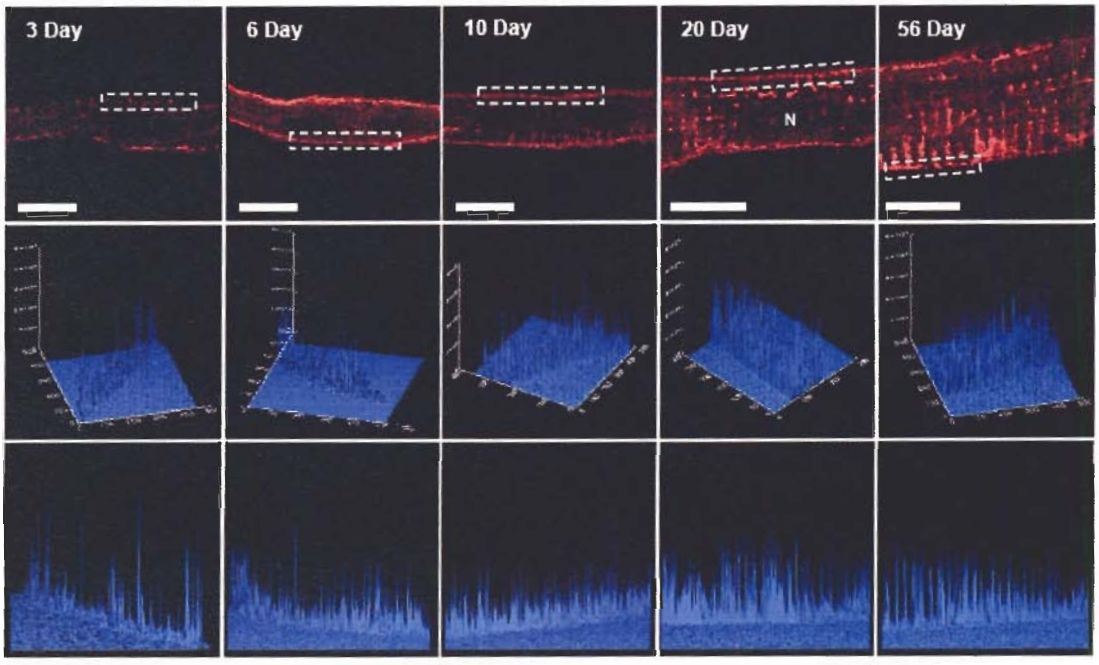

Figure 9. Developmental Changes in NCX Immunostaining Pattern.

Confocal images of a single optical slice from the middle of a representative cell from each age group(top panel). The intensity profile of the whole cell and the selected area are shown below for each panel (middle and bottom panels). Scale bars equal 5 μm

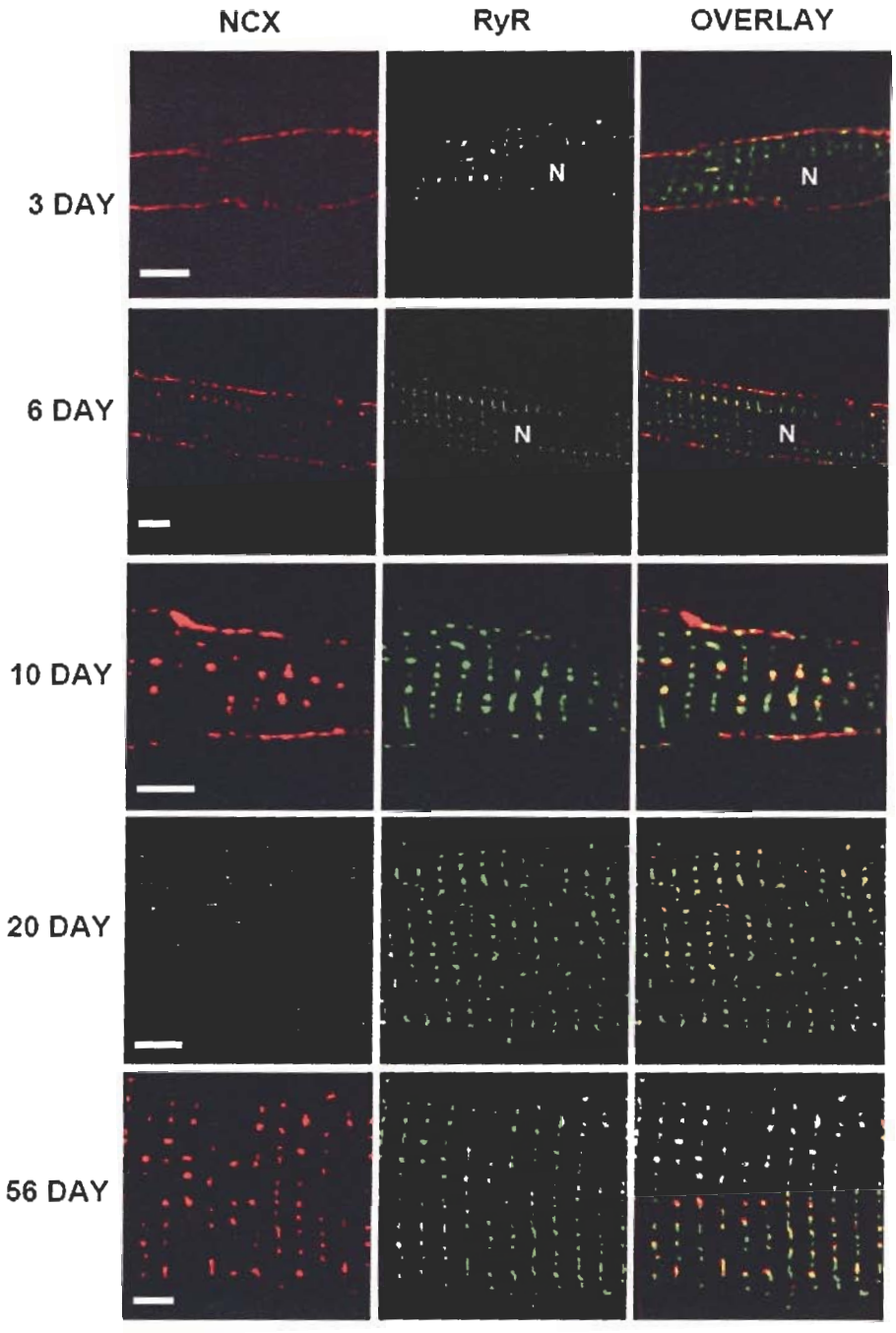

Figure 10. Colocalization Staining Pattern During Development

The colocalization staining pattern (left, pseudo-coloured yellow) is shown in myocardial cells isolated from 3-20 day old rabbits. NCX and RyR immunostaining are also shown (right and middle) and have been pseudo coloured in red and green respectively. Scale bars equal 5 μm

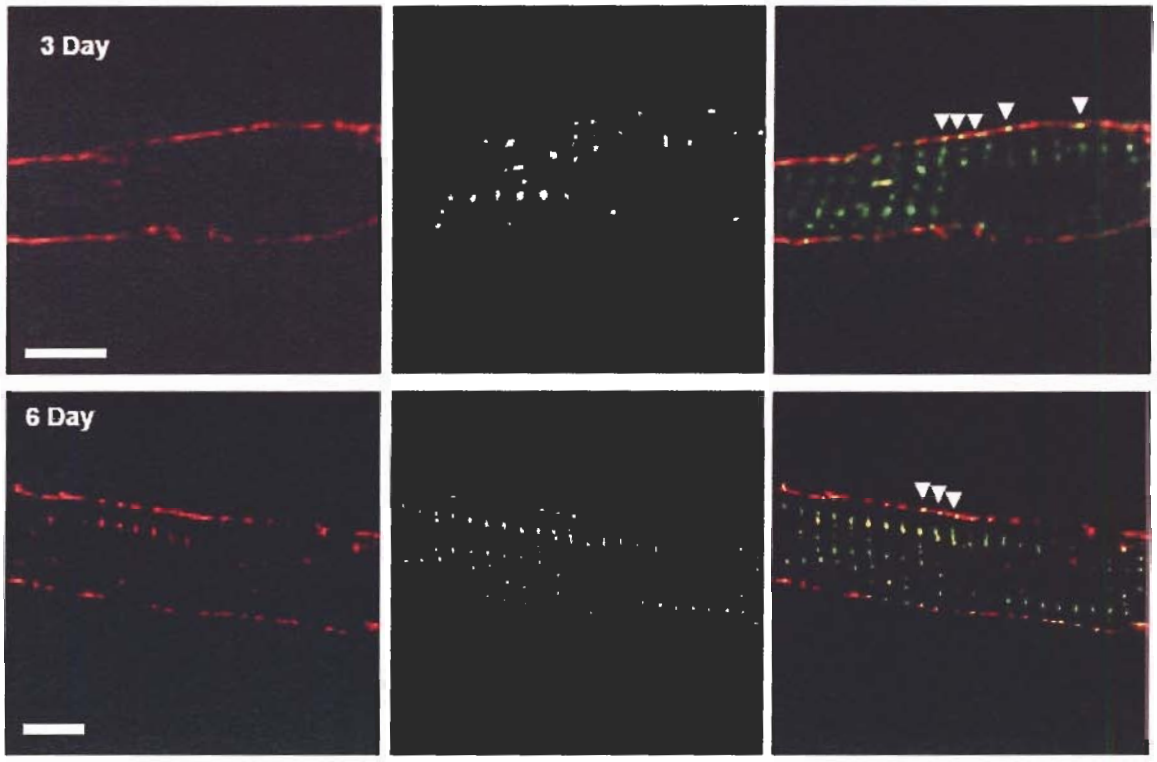

Figure 11. Colocalization Staining Pattern in 3- and 6-day old Myocytes

A close up of the colocalization staining pattern (left, pseudo-coloured yellow) is shown in myocardial cells isolated from 3- and 6-day old rabbits. NCX and RyR immunostaining are also shown (right and middle) and have been pseudo coloured in red and green respectively. Arrows point to colocalization occur at the junctions of RyR with the sarcolemma. Scale bars equal 5 μm

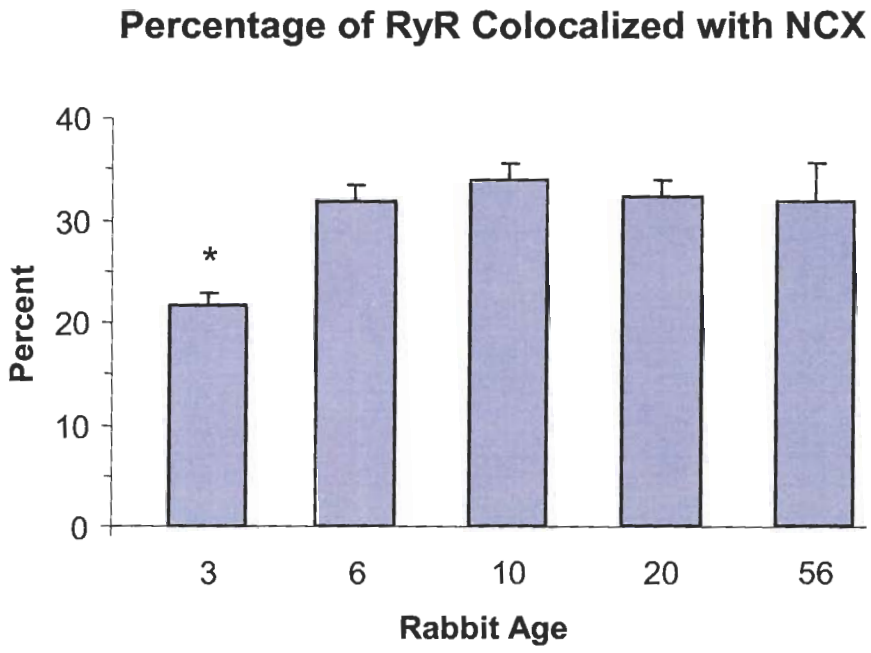

Figure 12. Degree of RyR Colocalization in Different Age Groups

Bar graphs represent the mean percentage of RyR colocalized with NCX in the different age groups. Degree of colocalization was calculated by dividing the total number of colocalized voxels with the total number of RyR Voxels. *Differs significantly from each other ($P < 0.0001$)

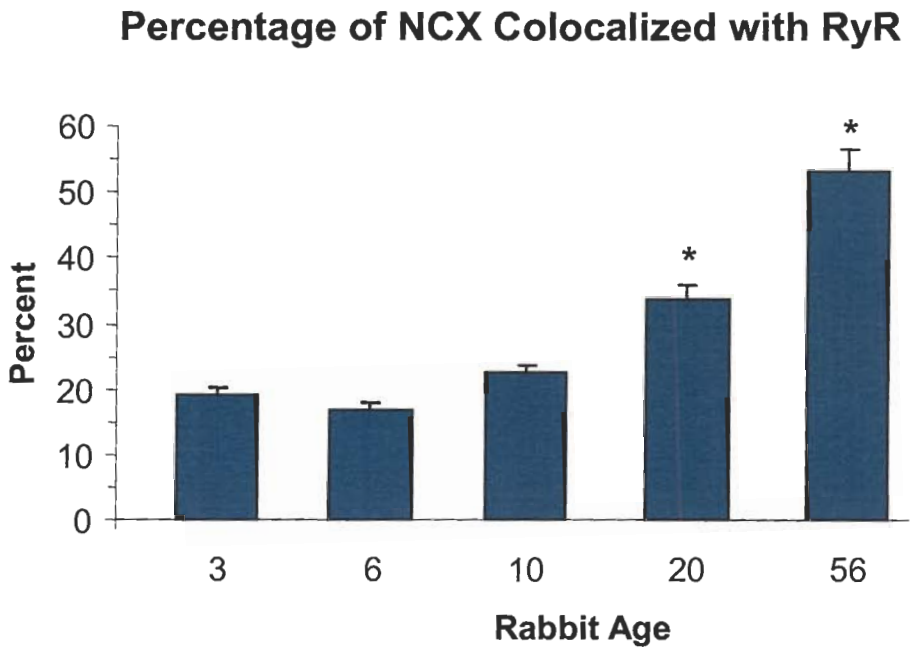

Figure 13. Degree of NCX Colocalization in Different Age Groups

Bar graphs represent the mean percentage of NCX colocalized with RyR in the different age groups. Degree of colocalization was calculated by dividing the total number of colocalized voxels with the total number of NCX Voxels. *Differs significantly from each other ($P < 0.0001$)

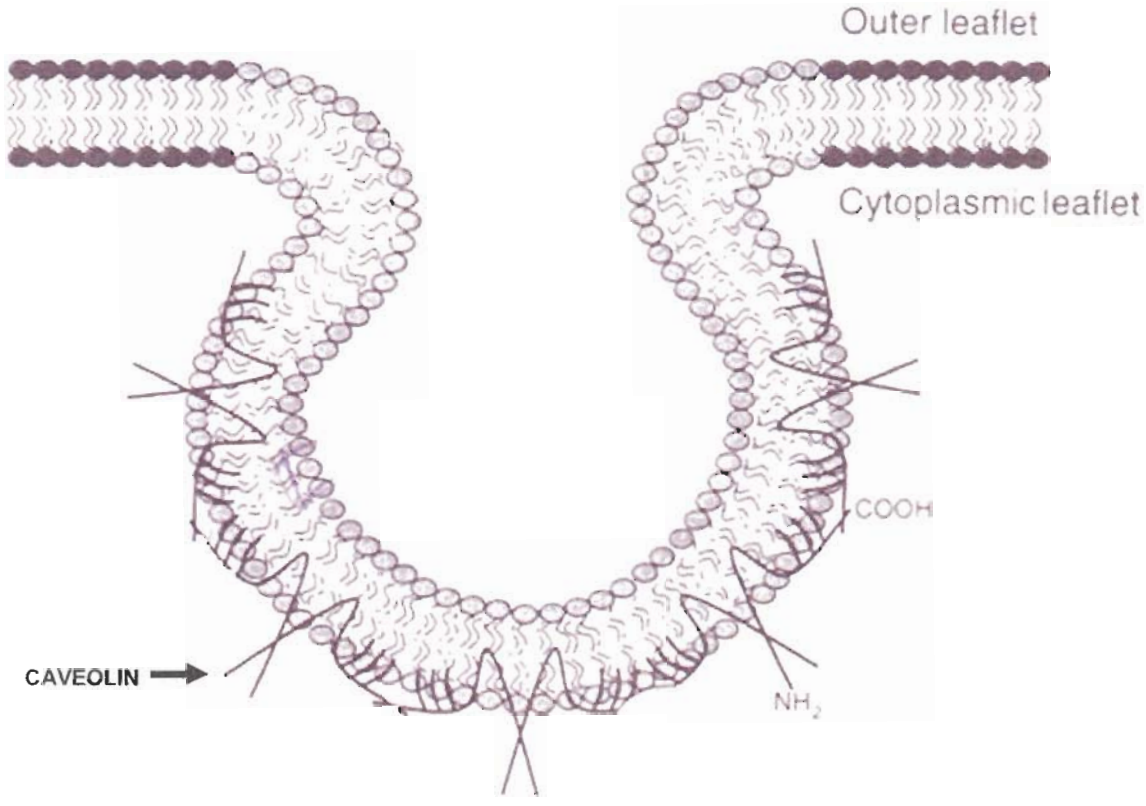

Figure 14. Schematic Representation of Caveolae

Model of the organization of caveolae, a specialized microdomain. Caveolae are formed through the self-association of caveolin molecules making a hairpin loop

REFERENCE LIST

Allan, V. J. (2000). "Protein localization by fluorescence microscopy : a practical approach." Oxford University Press,, Oxford, New York.

Anderson, K., Lai, F. A., Liu, Q. Y., Rousseau, E., Erickson, H. P., and Meissner, G. (1989). Structural and functional characterization of the purified cardiac ryanodine receptor-Ca^{2+} release channel complex. *J Biol Chem* **264,** 1329-35.

Artman, M. (1992). Sarcolemmal $Na^{(+)}$-Ca^{2+} exchange activity and exchanger immunoreactivity in developing rabbit hearts. *Am J Physiol Heart Circ Physiol* **263,** H1506-1513.

Artman, M., Henry, G., and Coetzee, W. A. (2000). Cellular basis for age-related differences in cardiac excitation-contraction coupling. *Progress in Pediatric Research* **11,** 185-194.

Artman, M., Ichikawa, H., Avkiran, M., and Coetzee, W. A. (1995). Na^{+}/Ca^{2+} exchange current density in cardiac myocytes from rabbits and guinea pigs during postnatal development. *Am J Physiol Heart Circ Physiol* **268,** H1714-1722.

Balaguru, D., Haddock, P. S., Puglisi, J. L., Bers, D. M., Coetzee, W. A., and Artman, M. (1997). Role of the sarcoplasmic reticulum in contraction and relaxation of immature rabbit ventricular myocytes. *J Mol Cell Cardiol* **29,** 2747-57.

Bassani, R. A., Shannon, T. R., and Bers, D. M. (1998). Passive Ca^{2+} binding in ventricular myocardium of neonatal and adult rats. *Cell Calcium* **23,** 433-42.

Benkusky, N. A., Farrell, E. F., and Valdivia, H. H. (2004). Ryanodine receptor channelopathies. *Biochem Biophys Res Commun* **322,** 1280-5.

Berne, R. M., Levy, M. N., Koeppen, B. M., and Stanton, B. A. (1998). "Physiology." Mosby, Inc, St. Louis.

Bers, D. M. (1991). Ca regulation in cardiac muscle. *Med Sci Sports Exerc* **23,** 1157-62.

Bers, D. M. (2001). "Excitation-Contraction Coupling and Cardiac Contractile Force." Kluwer Academic Publishers, Dordrecht.

Bers, D. M. (2002). Cardiac excitation-contraction coupling. *Nature* **415,** 198-205.

Bers, D. M. (2004). Macromolecular complexes regulating cardiac ryanodine receptor function. *J Mol Cell Cardiol* **37,** 417-29.

Bers, D. M., Lederer, W. J., and Berlin, J. R. (1990). Intracellular Ca transients in rat cardiac myocytes: role of Na-Ca exchange in excitation-contraction coupling. *Am J Physiol* **258,** C944-54.

Bers, D. M., and Stiffel, V. M. (1993). Ratio of ryanodine to dihydropyridine receptors in cardiac and skeletal muscle and implications for E-C coupling. *Am J Physiol* **264,** C1587-93.

Bossuyt, J., Taylor, B. E., James-Kracke, M., and Hale, C. C. (2002). The Cardiac Sodium-Calcium Exchanger Associates with Caveolin-3. *Ann N Y Acad Sci* **976,** 197-204.

Bradford, M. M. (1976). A rapid and sensitive method for the quantitation of microgram quantities of protein utilizing the principle of protein-dye binding. *Anal Biochem* **72,** 248-54.

Bullock, G. R., and Petrusz, P. (1982). Techniques in immunocytochemistry. Academic Press, London New York.

Burry, R. W. (2000). Specificity Controls for Immunocytochemical Methods. *J. Histochem. Cytochem.* **48,** 163-166.

Cai, X., and Lytton, J. (2004). The cation/$Ca^{(2+)}$ exchanger superfamily: phylogenetic analysis and structural implications. *Mol Biol Evol* **21,** 1692-703.

Callewaert, G. (1992). Excitation-contraction coupling in mammalian cardiac cells. *Cardiovasc Res* **26,** 923-32.

Cannell, M. B., Cheng, H., and Lederer, W. J. (1995). The Control of Calcium Release in Heart Muscle. *Science* **268,** 1045-1049.

Carl, S. L., Felix, K., Caswell, A. H., Brandt, N. R., Ball, W. J., Jr., Vaghy, P. L., Meissner, G., and Ferguson, D. G. (1995). Immunolocalization of sarcolemmal dihydropyridine receptor and sarcoplasmic reticular triadin and ryanodine receptor in rabbit ventricle and atrium. *J Cell Biol* **129,** 672-82.

Chen, F., Mottino, G., Klitzner, T. S., Philipson, K. D., and Frank, J. S. (1995). Distribution of the Na^+/Ca^{2+} exchange protein in developing rabbit myocytes. *Am J Physiol Cell Physiol* **268,** C1126-1132.

Cheng, H., Lederer, W. J., and Cannell, M. B. (1993). Calcium Sparks: Elementary Events Underlying Excitation-Contraction Coupling in Heart Muscle. *Science* **262,** 740-744.

Cherednichenko, G., Zima, A. V., Feng, W., Schaefer, S., Blatter, L. A., and Pessah, I. N. (2004). NADH oxidase activity of rat cardiac sarcoplasmic reticulum regulates calcium-induced calcium release. *Circ Res* **94,** 478-86.

Chin, T. K., Friedman, W. F., and Klitzner, T. S. (1990). Developmental changes in cardiac myocyte calcium regulation. *Circ Res* **67,** 574-9.

Cook, O., Low, W., and Rahamimoff, H. (1998). Membrane topology of the rat brain Na^+-Ca^{2+} exchanger. *Biochimica et Biophysica Acta (BBA) - Biomembranes* **1371,** 40-52.

Cox, G. (2002). Biological confocal microscopy. *Materials Today* **5,** 34-41.

Cox, G., and Sheppard, C. J. (2004). Practical limits of resolution in confocal and non-linear microscopy. *Microsc Res Tech* **63,** 18-22.

Dipla, K., Mattiello, J. A., Margulies, K. B., Jeevanandam, V., and Houser, S. R. (1999). The Sarcoplasmic Reticulum and the Na^+/Ca^{2+} Exchanger Both Contribute to the Ca^{2+} Transient of Failing Human Ventricular Myocytes. *Circ Res* **84,** 435-444.

Drevot, P., Langlet, C., Guo, X. J., Bernard, A. M., Colard, O., Chauvin, J. P., Lasserre, R., and He, H. T. (2002). TCR signal initiation machinery is pre-assembled and activated in a subset of membrane rafts. *Embo J* **21,** 1899-908.

Du, G. G., Sandhu, B., Khanna, V. K., Guo, X. H., and MacLennan, D. H. (2002). Topology of the Ca^{2+} release channel of skeletal muscle sarcoplasmic reticulum (RyR1). *PNAS* **99,** 16725-16730.

Fabiato, A. (1983). Calcium-induced release of calcium from the cardiac sarcoplasmic reticulum. *Am J Physiol* **245,** C1-14.

Feron, O., and Kelly, R. A. (2002). Gaining Respectability: Membrane-Delimited, Caveolar-Restricted Activation of Ion Channels. *Circ Res* **90,** 369-370.

Ferrier, G. R., and Howlett, S. E. (2001). Cardiac excitation-contraction coupling: role of membrane potential in regulation of contraction. *Am J Physiol Heart Circ Physiol* **280,** H1928-44.

Fill, M., and Copello, J. A. (2002). Ryanodine Receptor Calcium Release Channels. *Physiol. Rev.* **82,** 893-922.

Flucher, B. E., and Franzini Armstrong, C. (1996). Formation of junctions involved in excitation-contraction coupling in skeletal and cardiac muscle. *Proc Natl Acad Sci U S A* **93,** 8101-6.

Fozzard, H. A. (1991). Excitation-contraction coupling in the heart. *Adv Exp Med Biol* **308,** 135-42.

Frank, J. S., Mottino, G., Reid, D., Molday, R. S., and Philipson, K. D. (1992). Distribution of the $Na^{(+)}$-Ca^{2+} exchange protein in mammalian cardiac myocytes: an immunofluorescence and immunocolloidal gold-labeling study. *J Cell Biol* **117,** 337-45.

Franzini-Armstrong, C., Protasi, F., and Ramesh, V. (1999). Shape, Size, and Distribution of Ca^{2+} Release Units and Couplons in Skeletal and Cardiac Muscles. *Biophys. J.* **77,** 1528-1539.

Fujita, T., Toya, Y., Iwatsubo, K., Onda, T., Kimura, K., Umemura, S., and Ishikawa, Y. (2001). Accumulation of molecules involved in alpha1-adrenergic signal within caveolae: caveolin expression and the development of cardiac hypertrophy. *Cardiovasc Res* **51,** 709-16.

Grunwald, R., and Meissner, G. (1995). Lumenal sites and C terminus accessibility of the skeletal muscle calcium release channel (ryanodine receptor). *J Biol Chem* **270,** 11338-47.

Haddock, P. S., Coetzee, W. A., Cho, E., Porter, L., Katoh, H., Bers, D. M., Jafri, M. S., and Artman, M. (1999). Subcellular $[Ca^{2+}]_i$ gradients during excitation-contraction coupling in newborn rabbit ventricular myocytes. *Circ Res* **85,** 415-27.

Hakamata, Y., Nakai, J., Takeshima, H., and Imoto, K. (1992). Primary structure and distribution of a novel ryanodine receptor/calcium release channel from rabbit brain. *FEBS Letters* **312,** 229-235.

Hibbs, A. R. (2000). "Confocal Microscopy for Biologists: an Intensive Introductory Course." Bicon, Ringwood East.

Hilgemann, D. W. (2004). New insights into the molecular and cellular workings of the cardiac Na^+/Ca^{2+} exchanger. *Am J Physiol Cell Physiol* **287,** C1167-1172.

Hoerter, J., Mazet, F., and Vassort, G. (1981). Perinatal growth of the rabbit cardiac cell: possible implications for the mechanism of relaxation. *J Mol Cell Cardiol* **13,** 725-40.

Hoessli, D. C., Ilangumaran, S., Soltermann, A., Robinson, P. J., Borisch, B., and Nasir Ud, D. (2000). Signaling through sphingolipid microdomains of the plasma membrane: the concept of signaling platform. *Glycoconj J* **17,** 191-7.

Horackova, M. (1986). Excitation-contraction coupling in isolated adult ventricular myocytes from the rat, dog, and rabbit: effects of various inotropic interventions in the presence of ryanodine. *Can J Physiol Pharmacol* **64,** 1473-83.

Hryshko, L. V., Nicoll, D. A., Weiss, J. N., and Philipson, K. D. (1993). Biosynthesis and initial processing of the cardiac sarcolemmal Na^+-Ca^{2+} exchanger. *Biochimica et Biophysica Acta (BBA) - Biomembranes* **1151,** 35-42.

Huang, J., Hove-Madsen, L., and Tibbits, G. F. (2004). Na^+-Ca^{2+} exchange activity in neonatal rabbit ventricular myocytes. *Am J Physiol Cell Physiol* **18,** 18.

Huynh, T. V., Chen, F., Wetzel, G. T., Friedman, W. F., and Klitzner, T. S. (1992). Developmental changes in membrane Ca^{2+} and K^+ currents in fetal, neonatal, and adult rabbit ventricular myocytes. *Circ Res* **70,** 508-15.

Ilangumaran, S., Borisch, B., and Hoessli, D. C. (1999). Signal transduction via CD44: role of plasma membrane microdomains. *Leuk Lymphoma* **35,** 455-69.

Inui, M., Saito, A., and Fleischer, S. (1987). Isolation of the ryanodine receptor from cardiac sarcoplasmic reticulum and identity with the feet structures. *J Biol Chem* **262,** 15637-42.

Iwamoto, T., Nakamura, T. Y., Pan, Y., Uehara, A., Imanaga, I., and Shigekawa, M. (1999). Unique topology of the internal repeats in the cardiac Na^+/Ca^{2+} exchanger. *FEBS Letters* **446,** 264-268.

Jayaraman, T., Brillantes, A. M., Timerman, A. P., Fleischer, S., Erdjument-Bromage, H., Tempst, P., and Marks, A. R. (1992). FK506 binding protein associated with the calcium release channel (ryanodine receptor). *J Biol Chem* **267,** 9474-7.

Johnson, E. A., Lemieux, R. D., Hume, J. R., Levesque, P. C., Leblanc, N., Lederer, W. J., Niggli, E., and Hadley, R. W. (1991). Sodium-Calcium Exchange. *Science* **251,** 1370-1371.

Kieval, R. S., Bloch, R. J., Lindenmayer, G. E., Ambesi, A., and Lederer, W. J. (1992). Immunofluorescence localization of the Na-Ca exchanger in heart cells. *Am J Physiol Cell Physiol* **263,** C545-550.

Klitzner, T., and Friedman, W. F. (1988). Excitation-contraction coupling in developing mammalian myocardium: evidence from voltage clamp studies. *Pediatr Res* **23,** 428-32.

Klitzner, T. S., Chen, F. H., Raven, R. R., Wetzel, G. T., and Friedman, W. F. (1991). Calcium current and tension generation in immature mammalian myocardium: effects of diltiazem. *J Mol Cell Cardiol* **23,** 807-15.

Koban, M. U., Moorman, A. F. M., Holtz, J., Yacoub, M. H., and Boheler, K. R. (1998). Expressional analysis of the cardiac Na-Ca exchanger in rat development and senescence. *Cardiovascular Research* **37,** 405-423.

Kovarova, M., Tolar, P., Arudchandran, R., Draberova, L., Rivera, J., and Draber, P. (2001). Structure-function analysis of Lyn kinase association with lipid rafts and initiation of early signaling events after Fcepsilon receptor I aggregation. *Mol Cell Biol* **21,** 8318-28.

Landmann, L. (2002). Deconvolution improves colocalization analysis of multiple fluorochromes in 3D confocal data sets more than filtering techniques. *J Microsc* **208,** 134-47.

Langer, G. A. (1987). The role of calcium at the sarcolemma in the control of myocardial contractility. *Can J Physiol Pharmacol* **65,** 627-31.

Larson, J. (2002). 2D and 3D Deconvolution of Confocal Fluorescence Images by Maximum Likelihood Estimation. *In* "Three-Dimensional and Multidimensional Microscopy: Image Acquistion and Processing IX", Vol. 4621, pp. 1-11. Society of Photo-Optical Instrumentation Engineers, San Jose, USA.

Larsson, L.-I. (1988.). "Immunocytochemistry : theory and practice / author, Lars-Inge Larsson." CRC Press, c, Boca Raton, Fla.

Leblanc, N., and Hume, J. R. (1990). Sodium Current-Induced Release of Calcium from Cardiac Sarcoplasmic Reticulum. *Science* **248,** 372-376.

Lederer, W. J., Niggli, E., and Hadley, R. W. (1990). Sodium-Calcium Exchange in Excitable Cells: Fuzzy Space. *Science* **248,** 283.

Levesque, P. C., Leblanc, N., and Hume, J. R. (1991). Role of reverse-mode $Na^{(+)}$-Ca^{2+} exchange in excitation-contraction coupling in the heart. *Ann N Y Acad Sci* **639,** 386-97.

Li, Z., Matsuoka, S., Hryshko, L., Nicoll, D., Bersohn, M., Burke, E., Lifton, R., and Philipson, K. (1994). Cloning of the NCX2 isoform of the plasma membrane $Na^{(+)}$-Ca^{2+} exchanger. *J. Biol. Chem.* **269,** 17434-17439.

Lohn, M., Furstenau, M., Sagach, V., Elger, M., Schulze, W., Luft, F. C., Haller, H., and Gollasch, M. (2000). Ignition of Calcium Sparks in Arterial and Cardiac Muscle Through Caveolae. *Circ Res* **87,** 1034-1039.

Ma, J., Hayek, S. M., and Bhat, M. B. (2004). Membrane topology and membrane retention of the ryanodine receptor calcium release channel. *Cell Biochem Biophys* **40,** 207-24.

Malkusch, W., Bauch, H., and Schafer, L. (2001). Digital light microscopy: Prerequisite for optimum contrast enhancement and increase of resolution. *Experimental Gerontology* **36,** 1199-1217.

Marks, A. R. (2001). Ryanodine receptors/calcium release channels in heart failure and sudden cardiac death. *J Mol Cell Cardiol* **33,** 615-24.

Marshall, C. R., Pan, T. C., Le, H. D., Omelchenko, A., Hwang, P. P., Hryshko, L. V., and Tibbits, G. F. (2005). cDNA cloning and expression of cardiac Na^{+}/Ca^{2+} exchanger (NCX) from mozambique tilapia (Oreochromis Mossambicus) reveals teleost membrane transporter with mammalian temperature dependence. *J Biol Chem.*

Matsuoka, S., Nicoll, D., Reilly, R., Hilgemann, D., and Philipson, K. (1993). Initial Localization of Regulatory Regions of the Cardiac Sarcolemmal Na^{+}-Ca^{2+} Exchanger. *PNAS* **90,** 3870-3874.

Mayrleitner, M., Timerman, A. P., Wiederrecht, G., and Fleischer, S. (1994). The calcium release channel of sarcoplasmic reticulum is modulated by FK-506 binding protein: effect of FKBP-12 on single channel activity of the skeletal muscle ryanodine receptor. *Cell Calcium* **15,** 99-108.

McDonough, A. A., Velotta, J. B., Schwinger, R. H., Philipson, K. D., and Farley, R. A. (2002). The cardiac sodium pump: structure and function. *Basic Res Cardiol* **97,** I19-24.

McNally, J. G., Karpova, T., Cooper, J., and Conchello, J. A. (1999). Three-Dimensional Imaging by Deconvolution Microscopy. *Methods* **19,** 373-385.

Meissner, G. (2004). NADH, a new player in the cardiac ryanodine receptor? *Circ Res* **94,** 418-9.

Meissner, G., Rousseau, E., Lai, F. A., Liu, Q. Y., and Anderson, K. A. (1988). Biochemical characterization of the Ca^{2+} release channel of skeletal and cardiac sarcoplasmic reticulum. *Mol Cell Biochem* **82,** 59-65.

Moore, E. D. W., Etter, E. F., Philipson, K. D., Carrington, W. A., Fogarty, K. E., Lifshitz, L. M., and Fay, F. S. (1993). Coupling of the Na+/Ca2+exchanger, Na+/K+ pump and sarcoplasmic reticulum in smooth muscle. **365,** 657-660.

Nabauer, M., Callewaert, G., Cleemann, L., and Morad, M. (1989). Regulation of calcium release is gated by calcium current, not gating charge, in cardiac myocytes. *Science* **244,** 800-3.

Nakai, J., Imagawa, T., Hakamat, Y., Shigekawa, M., Takeshima, H., and Numa, S. (1990). Primary structure and functional expression from cDNA of the cardiac ryanodine receptor/calcium release channel. *FEBS Lett* **271,** 169-77.

Nicoll, D. A., Longoni, S., and Philipson, K. D. (1990). Molecular cloning and functional expression of the cardiac sarcolemmal $Na^{(+)}$-Ca^{2+} exchanger. *Science* **250,** 562-5.

Nicoll, D. A., Ottolia, M., Lu, L., Lu, Y., and Philipson, K. D. (1999). A New Topological Model of the Cardiac Sarcolemmal Na^{+}-Ca^{2+} Exchanger. *J. Biol. Chem.* **274,** 910-917.

Nicoll, D. A., Quednau, B. D., Qui, Z., Xia, Y.-R., Lusis, A. J., and Philipson, K. D. (1996). Cloning of a Third Mammalian Na+-Ca2+ Exchanger, NCX3. *J. Biol. Chem.* **271,** 24914-24921.

Niggli, E., and Lederer, W. J. (1990). Voltage-independent calcium release in heart muscle. *Science* **250,** 565-8.

Noorden, J. M. P. a. S. V. (1983.). "Immunocytochemistry : practical applications in pathology and biology." Wright-PSG, Bristol ; Boston.

Okamoto, T., Schlegel, A., Scherer, P. E., and Lisanti, M. P. (1998). Caveolins, a family of scaffolding proteins for organizing "preassembled signaling complexes" at the plasma membrane. *J Biol Chem* **273,** 5419-22.

Paddock, S. W. (1999). Confocal laser scanning microscopy. *Biotechniques* **27,** 992-6, 998-1002, 1004.

Page, E. (1978). Quantitative ultrastructural analysis in cardiac membrane physiology. *Am J Physiol Cell Physiol* **235,** C147-158.

Parton, R. G., Way, M., Zorzi, N., and Stang, E. (1997). Caveolin-3 associates with developing T-tubules during muscle differentiation. *J Cell Biol* **136,** 137-54.

Pawley, J. B. (1995). "Handbook of Biological Confocal Microscopy." Plenum Press, New York.

Perez, C. G., Copello, J. A., Li, Y., Karko, K. L., Gomez, L., Ramos-Franco, J., Fill, M., Escobar, A. L., and Mejia-Alvarez, R. (2005). Ryanodine receptor function in newborn rat heart. *Am J Physiol Heart Circ Physiol* **288,** H2527-2540.

Petrusz, G. R. B. a. P. (1982). "Techniques in immunocytochemistry." Academic Press, London ; New York.

Philipson, K. D., and Nicoll, D. A. (2000). Sodium-Calcium Exchange: A Molecular Perspective. *Annual Review of Physiology* **62,** 111-133.

Pierce, G. N., Rich, T. L., and Langer, G. A. (1987). Trans-sarcolemmal Ca^{2+} movements associated with contraction of the rabbit right ventricular wall. *Circ Res* **61,** 805-14.

Polak, J. M. a. S. V. N. (2003.). "Introduction to immunocytochemistry." BIOS Scientific Publishers, Oxford.

Porzig, H., Li, Z., Nicoll, D. A., and Philipson, K. D. (1993). Mapping of the cardiac sodium-calcium exchanger with monoclonal antibodies. *Am J Physiol* **265,** C748-56.

Protasi, F., Sun, X.-H., and Franzini-Armstrong, C. (1996). Formation and Maturation of the Calcium Release Apparatus in Developing and Adult Avian Myocardium. *Developmental Biology* **173,** 265-278.

Qu, Y., and Boutjdir, M. (2001). Gene expression of SERCA2a and L- and T-type Ca channels during human heart development. *Pediatr Res* **50,** 569-74.

Qu, Y., Ghatpande, A., el-Sherif, N., and Boutjdir, M. (2000). Gene expression of Na^+/Ca^{2+} exchanger during development in human heart. *Cardiovasc Res* **45,** 866-73.

Radermacher, M., Rao, V., Grassucci, R., Frank, J., Timerman, A., Fleischer, S., and Wagenknecht, T. (1994). Cryo-electron microscopy and three-dimensional reconstruction of the calcium release channel/ryanodine receptor from skeletal muscle. *J. Cell Biol.* **127,** 411-423.

Schaart, G., Moens, L., Endert, J. M., and Ramaekers, F. C. S. (1997). Biochemical characterization of cardiotin, a sarcoplasmic reticulum associated protein. *FEBS Letters* **403,** 168-172.

Schrader, M., Hell, S. W., and van der Voort, H. T. M. (1996). Potential of confocal microscopes to resolve in the 50-100 nm range. *Applied Physics Letters* **69,** 3644-6.

Schwarz, E. M., and Benzer, S. (1997). Calx, a Na-Ca exchanger gene of Drosophila melanogaster. *PNAS* **94,** 10249-10254.

Scriven, D. R., Dan, P., and Moore, E. D. (2000). Distribution of proteins implicated in excitation-contraction coupling in rat ventricular myocytes. *Biophys J* **79,** 2682-91.

Scriven, D. R., Klimek, A., Lee, K. L., and Moore, E. D. (2002). The Molecular Architecture of Calcium Microdomains in Rat Cardiomyocytes. *Ann N Y Acad Sci* **976,** 488-499.

Sedarat, F. (1999). Immulocalization of Dihydropyridine and Ryanodine Receptors in Developing Rabbit Myocytes Using 3-Dimensional Microscopy. *In* "School of Kinesiology", pp. 91. Simon Fraser University, Burnaby.

Sedarat, F., Lin, E., Moore, E. D. W., and Tibbits, G. F. (2004). Deconvolution of confocal images of dihydropyridine and ryanodine receptors in developing cardiomyocytes. *J Appl Physiol* **97,** 1098-1103.

Sedarat, F., Xu, L., Moore, E. D., and Tibbits, G. F. (2000). Colocalization of dihydropyridine and ryanodine receptors in neonate rabbit heart using confocal microscopy. *Am J Physiol Heart Circ Physiol* **279,** H202-9.

Shah, P. K., and Sowdhamini, R. (2001). Structural understanding of the transmembrane domains of inositol triphosphate receptors and ryanodine receptors towards calcium channeling. *Protein Eng.* **14,** 867-874.

Shigekawa, M., and Iwamoto, T. (2001). Cardiac Na^+-Ca^{2+} Exchange : Molecular and Pharmacological Aspects. *Circ Res* **88,** 864-876.

Simons, K., and Ikonen, E. (1997). Functional rafts in cell membranes. *Nature* **387,** 569-72.

Song, K. S., Scherer, P. E., Tang, Z., Okamoto, T., Li, S., Chafel, M., Chu, C., Kohtz, D. S., and Lisanti, M. P. (1996). Expression of caveolin-3 in skeletal, cardiac, and smooth muscle cells. Caveolin-3 is a component of the sarcolemma and co-fractionates with dystrophin and dystrophin-associated glycoproteins. *J Biol Chem* **271,** 15160-5.

Sperelakis, N. (2001). Heart physiology and pathophysiology (Y. Kurachi, A. Terzic, M. V. Cohen, and N. Sperelakis, Eds.), pp. 1261. Academic Press, San Diego.

Stern, M. D. (1992). Theory of excitation-contraction coupling in cardiac muscle. *Biophys J* **63,** 497-517.

Takeshima, H., Nishimura, S., Matsumoto, T., Ishida, H., Kangawa, K., Minamino, N., Matsuo, H., Ueda, M., Hanaoka, M., Hirose, T., and et al. (1989). Primary structure and expression from complementary DNA of skeletal muscle ryanodine receptor. *Nature* **339,** 439-45.

Tang, Z., Scherer, P. E., Okamoto, T., Song, K., Chu, C., Kohtz, D. S., Nishimoto, I., Lodish, H. F., and Lisanti, M. P. (1996). Molecular cloning of caveolin-3, a novel member of the caveolin gene family expressed predominantly in muscle. *J Biol Chem* **271,** 2255-61.

Tibbits, G. F., Xu, L., and Sedarat, F. (2002). Ontogeny of excitation-contraction coupling in the mammalian heart. *Comparative Biochemistry and Physiology - Part A: Molecular & Integrative Physiology* **132,** 691-698.

Timerman, A. P., Jayaraman, T., Wiederrecht, G., Onoue, H., Marks, A. R., and Fleischer, S. (1994). The ryanodine receptor from canine heart sarcoplasmic reticulum is associated with a novel FK-506 binding protein. *Biochem Biophys Res Commun* **198,** 701-6.

Tunwell, R. E., Wickenden, C., Bertrand, B. M., Shevchenko, V. I., Walsh, M. B., Allen, P. D., and Lai, F. A. (1996). The human cardiac muscle ryanodine receptor-calcium release channel: identification, primary structure and topological analysis. *Biochem J* **318 (Pt 2),** 477-87.

Valdeolmillos, M., O'Neill, S. C., Smith, G. L., and Eisner, D. A. (1989). Calcium-induced calcium release activates contraction in intact cardiac cells. *Pflugers Arch* **413,** 676-8.

Viatchenko-Karpinski, S., Terentyev, D., Jenkins, L. A., Lutherer, L. O., and Gyorke, S. (2005). Synergistic Interactions between Ca^{2+} Entries through L-Type Ca^{2+} Channels and Na^{+}-Ca^{2+} Exchanger in Normal and Failing Heart. *J Physiol.*

Wallace, W., Schaefer, L. H., and Swedlow, J. R. (2001). A workingperson's guide to deconvolution in light microscopy. *Biotechniques* **31,** 1076-8, 1080, 1082 passim.

Wang, S.-Q., Wei, C., Zhao, G., Brochet, D. X. P., Shen, J., Song, L.-S., Wang, W., Yang, D., and Cheng, H. (2004). Imaging Microdomain Ca^{2+} in Muscle Cells. *Circ Res* **94,** 1011-1022.

Weber, C. R., Ginsburg, K. S., and Bers, D. M. (2003). Cardiac Submembrane [Na+] Transients Sensed by Na^{+}-Ca^{2+} Exchange Current. *Circ Res* **92,** 950-952.

Wetzel, G. T., Chen, F., and Klitzner, T. S. (1991). L- and T-type calcium channels in acutely isolated neonatal and adult cardiac myocytes. *Pediatr Res* **30,** 89-94.

Wetzel, G. T., Chen, F., and Klitzner, T. S. (1993). Ca^{2+} channel kinetics in acutely isolated fetal, neonatal, and adult rabbit cardiac myocytes. *Circ Res* **72,** 1065-74.

Wetzel, G. T., Chen, F., and Klitzner, T. S. (1995). Na^{+}/Ca^{2+} exchange and cell contraction in isolated neonatal and adult rabbit cardiac myocytes. *Am J Physiol Heart Circ Physiol* **268,** H1723-1733.

Wier, W. G., Beuckelmann, D. J., and Barcenas-Ruiz, L. (1988). $[Ca^{2+}]_i$ in single isolated cardiac cells: a review of recent results obtained with digital imaging microscopy and fura-2. *Can J Physiol Pharmacol* **66,** 1224-31.

Williams, A. J. (1997). The functions of two species of calcium channel in cardiac muscle excitation-contraction coupling. *Eur Heart J* **18,** A27-35.

Williams, A. J., West, D. J., and Sitsapesan, R. (2001). Light at the end of the $Ca^{(2+)}$-release channel tunnel: structures and mechanisms involved in ion translocation in ryanodine receptor channels. *Q Rev Biophys* **34,** 61-104.

Wong, A., Fabiato, A., and Bassingthwaighte, J. (1987). Model of Ca release mechanism from the sarcoplasmic reticulum: Ca-mediated activation, inactivation and reactivation. *In* "Electromechanical, Activation, Metabolism, and Perfusion of the Heart: Simulation and Experimental Models" (S. Sideman and R. Beyar, Eds.), Dordrecht.

Xu, X., Bittman, R., Duportail, G., Heissler, D., Vilcheze, C., and London, E. (2001). Effect of the structure of natural sterols and sphingolipids on the formation of ordered sphingolipid/sterol domains (rafts). Comparison of cholesterol to plant, fungal, and disease-associated sterols and comparison of sphingomyelin, cerebrosides, and ceramide. *J Biol Chem* **276,** 33540-6.

Yarbrough, T. L., Lu, T., Lee, H. C., and Shibata, E. F. (2002). Localization of cardiac sodium channels in caveolin-rich membrane domains: regulation of sodium current amplitude. *Circ Res* **90,** 443-9.

Zorzato, F., Fujii, J., Otsu, K., Phillips, M., Green, N., Lai, F., Meissner, G., and MacLennan, D. (1990). Molecular cloning of cDNA encoding human and rabbit forms of the Ca^{2+} release channel (ryanodine receptor) of skeletal muscle sarcoplasmic reticulum. *J. Biol. Chem.* **265,** 2244-2256.